3. A. Lanzavecchia, F. Sallusto, *Nat. Rev. Immunol.* **2**, 982 (2002).
4. I. C. MacLennan, *Annu. Rev. Immunol.* **12**, 117 (1994).
5. A. Strasser, P. J. Jost, S. Nagata, *Immunity* **30**, 180 (2009).
6. Y. Takahashi, H. Ohta, T. Takemori, *Immunity* **14**, 181 (2001).
7. Z. Hao *et al.*, *Immunity* **29**, 615 (2008).
8. Y. Takahashi *et al.*, *J. Exp. Med.* **190**, 399 (1999).
9. K. G. Smith, U. Weiss, K. Rajewsky, G. J. Nossal, D. M. Tarlinton, *Immunity* **1**, 803 (1994).
10. K. G. Smith *et al.*, *J. Exp. Med.* **191**, 475 (2000).
11. S. F. Fischer *et al.*, *Blood* **110**, 3978 (2007).
12. Materials and methods are available as supporting material on *Science* Online.
13. U. Klein *et al.*, *Proc. Natl. Acad. Sci. U.S.A.* **100**, 2639 (2003).
14. T. Yokoyama *et al.*, *Immunol. Lett.* **81**, 107 (2002).
15. K. Kwon *et al.*, *Immunity* **28**, 751 (2008).
16. M. Muramatsu *et al.*, *Cell* **102**, 553 (2000).
17. N. Motoyama *et al.*, *Science* **267**, 1506 (1995).
18. K. U. Wagner *et al.*, *Development* **127**, 4949 (2000).
19. A. Ridderstad, D. M. Tarlinton, *J. Immunol.* **160**, 4688 (1998).
20. A. Radbruch *et al.*, *Nat. Rev. Immunol.* **6**, 741 (2006).
21. K. G. Smith, A. Light, G. J. Nossal, D. M. Tarlinton, *EMBO J.* **16**, 2996 (1997).
22. E. M. Carrington *et al.*, *Proc. Natl. Acad. Sci. U.S.A.* **107**, 10967 (2010).
23. J. M. Adams, S. Cory, *Oncogene* **26**, 1324 (2007).
24. L. Chen *et al.*, *Mol. Cell* **17**, 393 (2005).
25. S. N. Willis *et al.*, *Science* **315**, 856 (2007).
26. H. Toyama *et al.*, *Immunity* **17**, 329 (2002).
27. J. Roes, K. Rajewsky, *J. Exp. Med.* **177**, 45 (1993).
28. D. Allen, T. Simon, F. Sablitzky, K. Rajewsky, A. Cumano, *EMBO J.* **7**, 1995 (1988).
29. A. Cumano, K. Rajewsky, *EMBO J.* **5**, 2459 (1986).
30. J. T. Opferman *et al.*, *Nature* **426**, 671 (2003).
31. C. D. Allen, T. Okada, J. G. Cyster, *Immunity* **27**, 190 (2007).
32. D. Tarlinton, *Nat. Rev. Immunol.* **6**, 785 (2006).
33. T. Oltersdorf *et al.*, *Nature* **435**, 677 (2005).
34. J. H. Cho-Vega *et al.*, *Hum. Pathol.* **35**, 1095 (2004).
35. D. Allen *et al.*, *Immunol. Rev.* **96**, 5 (1987).
36. This work was supported in part by grants from the National Health and Medical Research Council (NHMRC) Australia (356202 to D.M.T. and S.L.N. and 461221 to P.B. and A.S.), the Leukemia and Lymphoma Society (SCOR grant 7413), and the NIH (CA43540 and CA80188). D.M.T. and A.S. are supported by fellowships from the NHMRC; S.L.N. by a Pfizer Australia Research Fellowship; I.V. by the Olle Engkvist Byggmastare and Wenner-Gren Foundations; K.L. by a fellowship from the German Academic Exchange Service; P.B. by the Charles and Sylvia Viertel Charitable Foundation; and M.B. by Boehringer Ingelheim. DNA sequence data are available in GenBank (accession number HM804028-HM804084). We are indebted to the facilities of our respective institutes, particularly those responsible for animal husbandry and flow cytometry. We also acknowledge the assistance of L. O'Reilly for Western blot antibodies and the many helpful discussions with members of the Walter and Eliza Hall Institute B Cell Program. Author contributions are as follows: I.V. and D.M.T. designed the research; I.V., K.L., S.G., V.P., S.C., and P.J. performed experiments and contributed to interpretation and discussion; M.B., P.B., A.S., and S.L.N. contributed to the design of experiments, interpretation of results, and drafting the manuscript; I.V., K.L., and V.P. analyzed data and prepared figures; and I.V. and D.M.T. wrote the manuscript.

Interdependence of Cell Growth and Gene Expression: Origins and Consequences

Matthew Scott,[1]*† Carl W. Gunderson,[2]* Eduard M. Mateescu,[1] Zhongge Zhang,[2] Terence Hwa[1,2]‡

In bacteria, the rate of cell proliferation and the level of gene expression are intimately intertwined. Elucidating these relations is important both for understanding the physiological functions of endogenous genetic circuits and for designing robust synthetic systems. We describe a phenomenological study that reveals intrinsic constraints governing the allocation of resources toward protein synthesis and other aspects of cell growth. A theory incorporating these constraints can accurately predict how cell proliferation and gene expression affect one another, quantitatively accounting for the effect of translation-inhibiting antibiotics on gene expression and the effect of gratuitous protein expression on cell growth. The use of such empirical relations, analogous to phenomenological laws, may facilitate our understanding and manipulation of complex biological systems before underlying regulatory circuits are elucidated.

Systems biology is as an integrative approach to connect molecular-level mechanisms to cell-level behavior (*1*). Many studies have characterized the impact of molecular circuits and networks on cellular physiology (*1*, *2*), but less is known about the impact of cellular physiology on the functions of molecular networks (*3*–*5*). Endogenous and synthetic genetic circuits can be strongly affected by the physiological states of the organism, resulting in unpredictable outcomes (*4*, *6*–*8*). Consequently, both the understanding and implementation of molecular control are predicated on distinguishing global physiological constraints from specific regulatory interactions.

For bacterial cells under steady-state exponential growth, the rate of cell proliferation (the "growth rate") is an important characteristic of the physiological state. It is well known that the macromolecular composition (e.g., the mass fractions of protein, RNA, and DNA) of bacterial cells under exponential growth depends on the growth medium predominantly through the growth rate allowed by the nutritional content of the medium (*9*, *10*). Such growth rate dependencies inevitably affect the expression of individual genes (*4*, *11*) because protein synthesis is directly dependent on the cell's ribosome content. The latter is reflected by the RNA/protein ratio. In *Escherichia coli*, most of the RNA (~85%) is rRNA folded in ribosomes (*10*, *11*). A predictive understanding of the impact of growth physiology on gene expression therefore first requires an understanding of the cell's allocation of cellular resources to ribosome synthesis

(manifested by the RNA/protein ratio) at different growth rates.

For exponentially growing *E. coli* cells (*10*, *12*), the RNA/protein ratio r is linearly correlated with the specific growth rate λ [= (ln 2)/doubling time] (Fig. 1A). The correlation is described mathematically as

$$r = r_0 + \frac{\lambda}{\kappa_t} \qquad (1)$$

where r_0 is the vertical intercept and κ_t is the inverse of the slope (table S1). This linear correlation holds for various *E. coli* strains growing in medium that supports fast to moderately slow growth [e.g., 20 min to ~2 hours per doubling (*11*)], and it appears to be quite universal; similar linear correlations have been observed in many other microbes, including slow-growing unicellular eukaryotes (fig. S1). As suggested long ago from mass-balance considerations (*11*) and elaborated in (*13*), this linear correlation is expected if the ribosomes are growth-limiting and are engaged in translation at a constant rate, with the phenomenological parameter κ_t predicted to be proportional to the rate of protein synthesis. Consistent with the prediction, data on RNA/protein ratios from slow-translation mutants of *E. coli* K-12 (triangles in Fig. 1B) also exhibited linear correlations with the growth rate λ, but with steeper slopes than the parent strain (circles), which have smaller κ_t. Moreover, the corresponding κ_t values correlated linearly with the directly measured speed of translational elongation (*14*) (Fig. 1B, inset). Consequently, we call κ_t the "translational capacity" of the organism.

Translation can be inhibited in a graded manner by exposing cells to sublethal doses of a translation-inhibiting antibiotic. The RNA/protein ratios obtained for wild-type cells grown in medium with a fixed nutrient source and various

[1]Center for Theoretical Biological Physics, Department of Physics, University of California, San Diego, La Jolla, CA 92093, USA. [2]Section of Molecular Biology, Division of Biological Sciences, University of California, San Diego, La Jolla, CA 92093, USA.

*These authors contributed equally to this work.
†Present address: Department of Applied Mathematics, University of Waterloo, Waterloo, Ontario N2L 3G1, Canada.
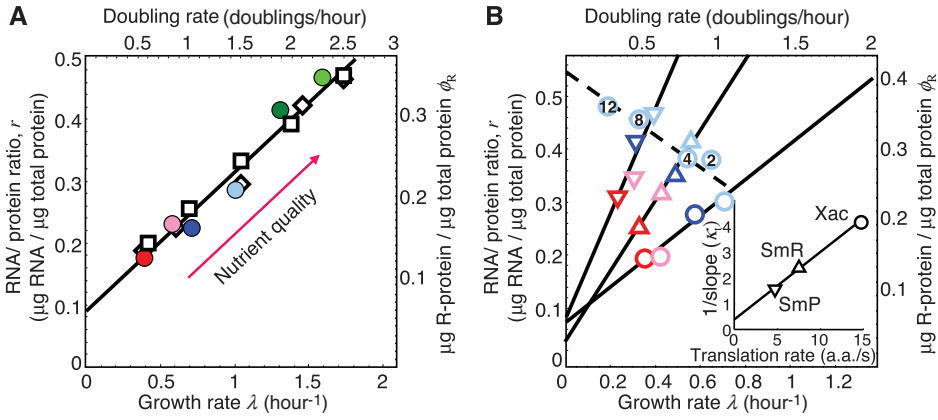‡To whom correspondence should be addressed. E-mail: hwa@ucsd.edu

Fig. 1. Correlation of the RNA/protein ratio r with growth rate λ for various strains of *E. coli*. (**A**) Comparison among *E. coli* strains grown in minimal medium: Strain B/r [(10), squares], 15τ-bar [(12), diamonds], and EQ2 (this work, solid circles). The growth rate is modulated by changing the quality of nutrients as indicated in the key at lower left. The fraction of total protein devoted to ribosome-affiliated proteins (ϕ_R) is given by the RNA/protein ratio as $\phi_R = \rho \cdot r$ (table S1). (**B**) The RNA/protein ratio for a family of translational mutants SmR (triangles) and SmP (inverted triangles) and their parent strain Xac (circles) (27), grown with various nutrients (see key at lower left) (table S2). Translational inhibition of the parent Xac strain via exposure to sublethal doses of chloramphenicol (circled numbers; see legend table) gave RNA/protein ratios similar to those of the mutant strains grown in medium with the same nutrient but without chloramphenicol (light blue symbols). Dashed line is a fit to Eq. 2. Inset: Linear correlation of κ_t values obtained for the Xac, SmR, and SmP strains (table S2) with the measured translation rate of the respective strains (14) ($r^2 = 0.99$).

amounts of chloramphenicol (Fig. 1B, light blue circles) were consistent with data obtained for the isogenic translational mutants grown in medium with the same nutrient but no antibiotic (light blue triangles). Surprisingly, these data revealed another linear correlation between r and λ (Fig. 1B, dashed line), given by

$$r = r_{max} - \frac{\lambda}{\kappa_n} \quad (2)$$

where r_{max} is the vertical intercept and κ_n is the inverse slope. Such a linear correlation was obtained for cells grown with each of the six nutrient sources studied (Fig. 2A and table S3). The correlation described by Eq. 2 has been observed in cells subjected to numerous other means of imposing translational limitation (fig. S2).

From Fig. 2A and the best-fit values of the parameters r_{max} and κ_n (table S4), we observed that the parameter κ_n exhibited a strong, positive correlation with the growth rate of cells in drug-free medium (fig. S3A). Thus, κ_n reflects the nutrient quality and is referred to as the "nutritional capacity" of the organism in a medium [see eq. S18 in (13) for a molecular interpretation of κ_n]. In contrast, the vertical intercept r_{max} depended only weakly on the composition of the growth medium (fig. S3B). Qualitatively, the increase of the RNA/protein ratio r with increasing degree of translational inhibition can be seen as a compensation for the reduced translational capacity, implemented possibly through the relief of repression of rRNA synthesis by the alarmone ppGpp (15), in response to the buildup of intracellular amino acid pools resulting from slow translation. Because r_{max} is the (extrapolated) maximal RNA/protein ratio as translation capacity is reduced toward zero, its weak dependence on the quality of the nutrients suggests a common
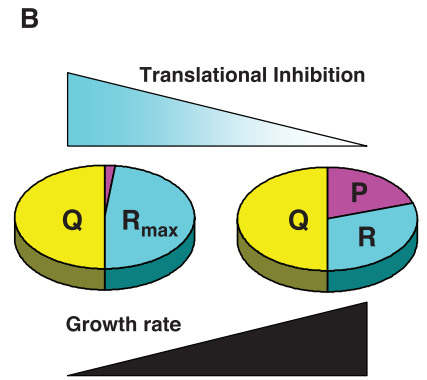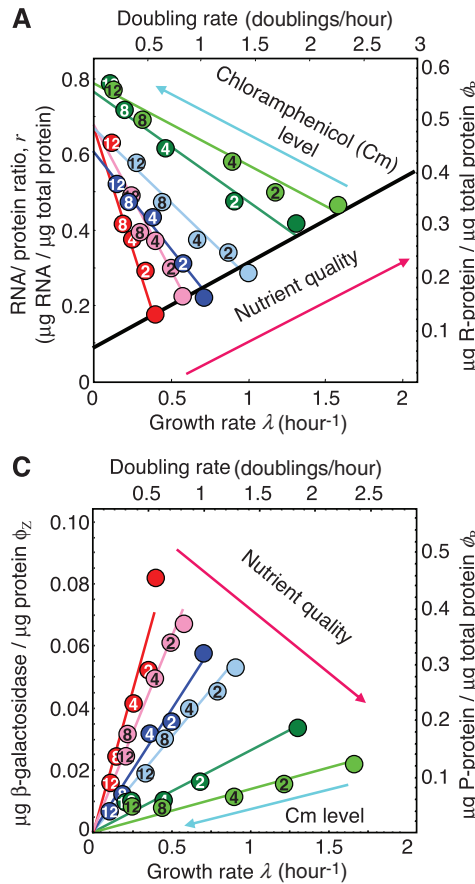

Fig. 2. Effect of translational inhibition. (**A**) RNA/protein ratio for strain EQ2 grown in different media, each with various levels of chloramphenicol (see key at lower right) (table S3). Solid lines were obtained from fitting data of the same color to Eq. 2. The black line describes the data in the absence of chloramphenicol (as in Fig. 1A). (**B**) Translational inhibition results in an increased synthesis of R-class proteins (cyan), effectively decreasing the fraction allocable to the P-class (magenta). (**C**) Mass fraction of constitutively expressed β-galactosidase (strain EQ3) plotted as a function of growth rate. The lines were fit according to Eq. 4. The growth rate dependence of constitutive gene expression due to nutrient limitation found in (4) is also well described by the theory (fig. S5C).
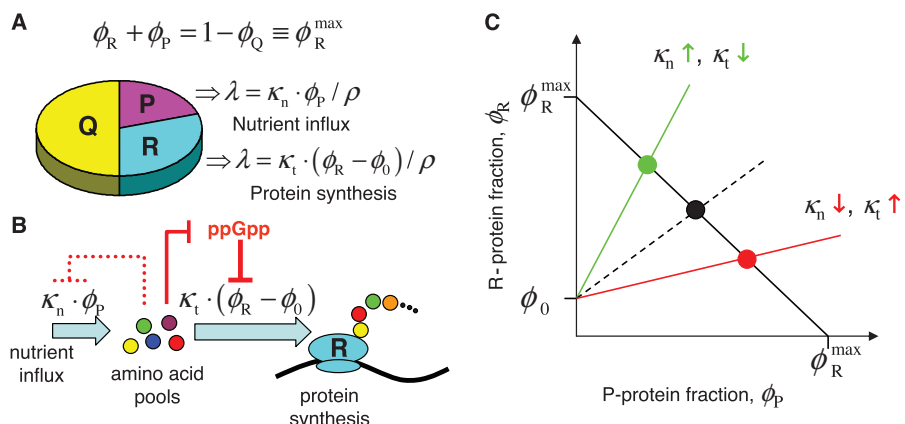
Fig. 3. A phenomenological theory of bacterial growth. (**A**) The growth theory comprises three key ingredients: (i) a three-component partition of the proteome, consisting of a fixed core sector (Q) and two adjustable sectors (R and P) whose fractions (ϕ_R and ϕ_P) must add up to a constant ($\phi_R^{max} = 1 - \phi_Q$); (ii) a ribosomal fraction ϕ_R containing all the ribosomal proteins and their affiliates and exerting a positive effect on growth (with growth rate $\lambda \propto \phi_R - \phi_0$, where $\phi_0 = \rho \cdot r_0$ corresponds to the vertical intercept in Fig. 1A); (iii) a remaining fraction ϕ_P exerting a similarly positive effect on growth (with growth rate $\lambda \propto \phi_P$) by providing an influx of nutrients (13). (**B**) During steady-state exponential growth, efficient resource allocation requires that the nutrient influx ($\kappa_n \cdot \phi_P$) be flux-matched to the amino acid outflux $\kappa_t \cdot (\phi_R - \phi_0)$. This can be coordinated by ppGpp, which up-regulates ribosome synthesis and hence amino acid outflux in response to increase in the amino acid pools, and has the opposite effect (down-regulating ribosome synthesis and hence amino acid outflux) in response to decrease in the amino acid pools (15). Changes in ϕ_R also indirectly regulate nutrient influx through the constraint of Eq. 3, in addition to direct regulatory mechanisms (dashed line). (**C**) Balancing the demands of protein synthesis and nutrient influx leads to the constraint ($\phi_R - \phi_0$)/$\phi_P = \kappa_n/\kappa_t$, sketched as the dashed black line. The other constraint (Eq. 3) is shown as the solid black line. The unique combination (ϕ_P, ϕ_R) satisfying both constraints is shown as the solid black circle. Upon increasing κ_n and/or decreasing κ_t, ϕ_R needs to be increased and ϕ_P decreased to maintain the balance (green line and circle), whereas with decreasing κ_n and/or increasing κ_t, ϕ_P needs to be increased and ϕ_R decreased (red line and symbols).

Fig. 4. Effect of unnecessary protein expression on growth. (**A**) Expression of an unnecessary protein (U) effectively decreases the fraction allocable to the R and P sectors, leading to a decrease in growth rate. (**B**) The growth defect caused by unnecessary protein expression in strain EQ30 (13). Data were collected from cells grown in three different media (same symbols as Fig. 2A) with various degrees of LacZ induction. The lines are predictions by Eq. 6, using the growth rate $\lambda(\phi_U = 0)$ and intercept $\phi_c = 0.48$ computed from the average r_{max} (table S4). (**C**) Comparison of unnecessary protein expression from various expression systems: β-lactamase driven by the σ^{70}-dependent *bla* promoter (open green circles) on a medium-copy plasmid (26), β-galactosidase driven by a T7 promoter (open red circles) or truncated EF-Tu driven by the σ^{70}-dependent *tac* promoter (open black circles), both on high-copy plasmids (19). β-Galactosidase driven by the σ^{54}-dependent P*u* promoter (solid blue circles) on a medium-copy plasmid [as in (B)] is shown for comparison.

limit in the allocation of cellular resources toward ribosome synthesis.

The simplest model connecting ribosome abundance to gene expression assumes that the total protein content of the cell (called the proteome) is composed of two classes: ribosome-affiliated "class R" proteins (with mass fraction ϕ_R), and "others" (with mass fraction $1 - \phi_R$) (5, 16). But the maximum allocation to the R-class proteins as derived from the value of r_{max}, $\phi_R^{max} = \rho \cdot r_{max} \approx 0.55$, is well below 1 [see (13) for the conversion factor ρ]. This suggests that the "other" proteins can be further subdivided minimally into two classes (Fig. 2B): "class Q" of mass fraction ϕ_Q, which is not affected translational inhibition, and the remainder, "class P" of mass fraction ϕ_P, with $\phi_P \to 0$ as $\phi_R \to \phi_R^{max}$(17). Because $\phi_P + \phi_Q + \phi_R = 1$, we must have $\phi_R^{max} = 1 - \phi_Q$, with

$$\phi_P = \phi_R^{max} - \phi_R = \rho \cdot (r_{max} - r) \qquad (3)$$

representing an important constraint between ϕ_P and ϕ_R. Together with Eq. 2, the model predicts

$$\phi_P = \rho \cdot \lambda / \kappa_n \qquad (4)$$

which describes a linear relation between the abundance of the P-class proteins and the growth rate λ for a fixed nutritional capacity κ_n. The growth rate independence of protein abundance may be maintained through negative autoregulation (4) (fig. S4). Unregulated (or "constitutively expressed") proteins belong instead to the P-class and can be used to test the prediction of Eq. 4: Expression of β-galactosidase driven by a constitutive promoter (ϕ_Z, mass of β-galactosidase per total protein mass) in cells grown under different degrees of chloramphenicol inhibition indeed correlated linearly with λ for each nutrient source studied (Fig. 2C), and the slopes of these correlations (colored lines) agree quantitatively with the nutritional capacity κ_n (fig. S5, A and B) as predicted by Eq. 4.

Although the correlations (Eqs. 2 and 4) were revealed by growth with antibiotics, their forms do not pertain specifically to translational inhibition. Equation 4 may be interpreted as a manifestation of P-class proteins providing the nutrients needed for growth [eqs. S15 to S18 in (13)], just as Eq. 1 is a reflection of R-class proteins providing the protein synthesis needed for growth (Fig. 3A). For different combinations of the nutritional and translational capacities (κ_n, κ_t), efficient resource allocation requires that the abundance of P- and R-class proteins be adjusted so that the rate of nutrient influx provided by P (via import or biosynthesis) matches the rate of protein synthesis achievable by R (Fig. 3B), while simultaneously satisfying the constraint of Eq. 3 (Fig. 3C). We can derive the resulting allocation mathematically by postulating that λ, ϕ_R (or r), and ϕ_P are analytical functions of the variables κ_t and κ_n that respectively capture all molecular details of translation and nutrition (analogous to state variables in thermodynamics). The mathematics
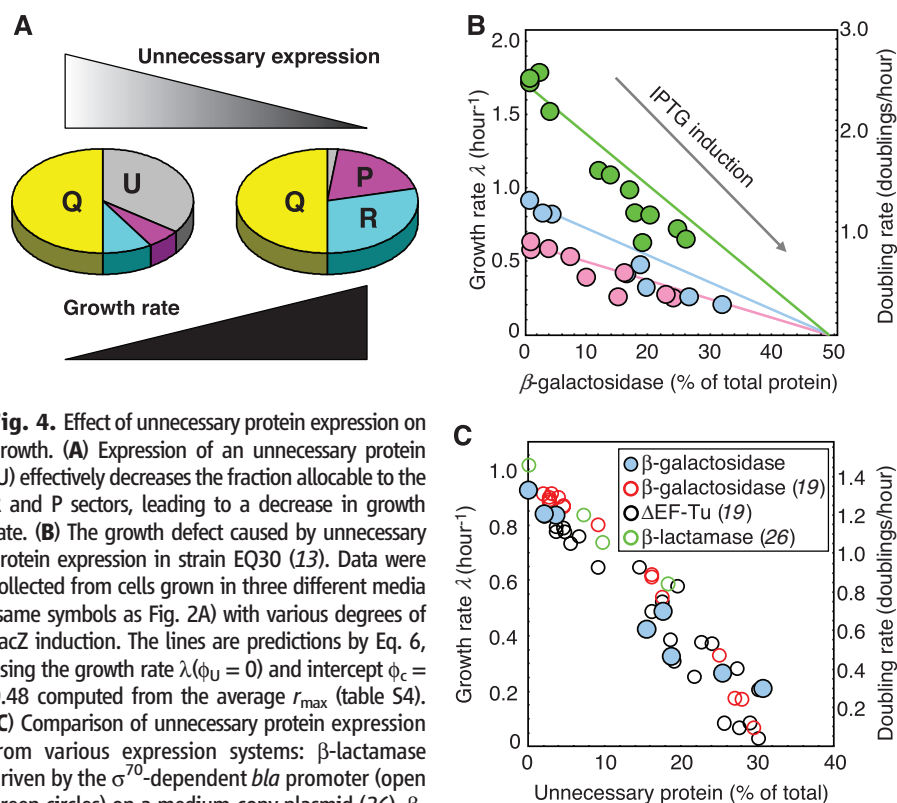
is identical to the description of an electric circuit with two resistors (fig. S6), with Eqs. 1 and 4 being analogous to Ohm's law. Solving these equations simultaneously leads to the Michaelis-Menten relation known empirically for the dependence of cell growth on nutrient level (*18*)

$$\lambda(\kappa_t, \kappa_n) = \lambda_c(\kappa_t) \cdot \frac{\kappa_n}{\kappa_t + \kappa_n} \qquad (5)$$

The value of the maximal growth rate $\lambda_c(\kappa_t) = \kappa_t \cdot (r_{max} - r_0) \approx 2.85 \, \text{hour}^{-1}$ (based on the average r_{max}) corresponds well to the doubling time of ~20 min for typical *E. coli* strains in rich media. Moreover, Eq. 5 quantitatively accounts for the correlation observed between growth rate λ and nutritional capacity κ_n (fig. S3A).

This theory can be inverted to predict the effect of protein expression on cell growth. Unnecessary protein expression leads to diminished growth (*19*). Understanding the origin of this growth inhibition is of value in efforts to increase the yield of heterologous protein in bacteria (*20*) and to understand the fitness benefit of gene regulation (*21*, *22*). Aside from protein-specific toxicity, several general causes of growth inhibition have been suggested, including diversion of metabolites (*23*), competition among sigma factors for RNA polymerases (*24*), and competition among mRNA for ribosomes (*19*, *25*).

We modeled the expression of unnecessary protein (of mass fraction ϕ_U) as an additional (neutral) component of the proteome that effectively causes a reduction of r_{max} to $r_{max} - \phi_U/\rho$ (Fig. 4A). Equation 5 then predicts a linear reduction of the growth rate,

$$\lambda(\phi_U) = \lambda(\phi_U = 0) \cdot [1 - (\phi_U/\phi_c)] \qquad (6)$$

extrapolating toward zero growth at $\phi_c = \rho \cdot (r_{max} - r_0) \approx 0.48$. The prediction quantitatively described the observed growth defect caused by inducible expression of β-galactosidase (Fig. 4B), as well as previous results obtained for various proteins and expression vectors (Fig. 4C) (*19*, *26*), without any adjustable parameters. These results suggest that growth reduction is a simple consequence of ribosome allocation subject to the constraints of Eqs. 1, 3, and 4.

Robust empirical correlations of the RNA/protein ratio with the growth rate (Figs. 1A and 2A and figs. S1 and S2) revealed underlying constraints of cellular resource allocation and led to the formulation of a simple growth theory that provided quantitative predictions and unifying descriptions of many important but seemingly unrelated aspects of bacterial physiology. Like Ohm's law, which greatly expedited the design of electrical circuits well before electricity was understood microscopically, the empirical correlations described here may be viewed as microbial "growth laws," the use of which may facilitate our understanding of the operation and design of complex biological systems well before all the underlying regulatory circuits are elucidated at the molecular level.

References and Notes

1. N. J. Guido *et al.*, *Nature* **439**, 856 (2006).
2. H. Youk, A. van Oudenaarden, *Nature* **462**, 875 (2009).
3. E. M. Airoldi *et al.*, *PLOS Comput. Biol.* **5**, e1000257 (2009).
4. S. Klumpp, Z. Zhang, T. Hwa, *Cell* **139**, 1366 (2009).
5. A. Zaslaver *et al.*, *PLOS Comput. Biol.* **5**, e1000545 (2009).
6. A. P. Arkin, D. A. Fletcher, *Genome Biol.* **7**, 114 (2006).
7. C. Tan, P. Marguet, L. You, *Nat. Chem. Biol.* **5**, 842 (2009).
8. R. Kwok, *Nature* **463**, 288 (2010).
9. M. Schaechter, O. Maaløe, N. O. Kjeldgaard, *J. Gen. Microbiol.* **19**, 592 (1958).
10. H. Bremer, P. P. Dennis, in *Escherichia coli and Salmonella*, F. C. Neidhardt, Ed. (ASM Press, Washington, DC, 1996), pp. 1553–1569.
11. O. Maaløe, in *Biological Regulation and Development*, R. F. Goldberger, Ed. (Plenum, New York, 1979), pp. 487–542.
12. J. Forchhammer, L. Lindahl, *J. Mol. Biol.* **55**, 563 (1971).
13. See supporting material on *Science* Online.
14. T. Ruusala, D. Andersson, M. Ehrenberg, C. G. Kurland, *EMBO J.* **3**, 2575 (1984).
15. B. J. Paul, W. Ross, T. Gaal, R. L. Gourse, *Annu. Rev. Genet.* **38**, 749 (2004).
16. A. L. Koch, *Can. J. Microbiol.* **34**, 421 (1988).
17. A particular protein species may belong to multiple classes; sometimes this is a result of expression from multiple promoters that are differently regulated.
18. J. Monod, *Annu. Rev. Microbiol.* **3**, 371 (1949).
19. H. Dong, L. Nilsson, C. G. Kurland, *J. Bacteriol.* **177**, 1497 (1995).
20. C. P. Chou, *Appl. Microbiol. Biotechnol.* **76**, 521 (2007).
21. E. Dekel, U. Alon, *Nature* **436**, 588 (2005).
22. D. M. Stoebel, A. M. Dean, D. E. Dykhuizen, *Genetics* **178**, 1653 (2008).
23. B. R. Glick, *Biotechnol. Adv.* **13**, 247 (1995).
24. A. Farewell, K. Kvint, T. Nyström, *Mol. Microbiol.* **29**, 1039 (1998).
25. J. Vind, M. A. Sørensen, M. D. Rasmussen, S. Pedersen, *J. Mol. Biol.* **231**, 678 (1993).
26. W. E. Bentley, N. Mirjalili, D. C. Andersen, R. H. Davis, D. S. Kompala, *Biotechnol. Bioeng.* **35**, 668 (1990).
27. R. Mikkola, C. G. Kurland, *Biochimie* **73**, 1551 (1991).
28. We thank H. Bremer, L. Csonka, P. Dennis, M. Ehrenberg, P. Geiduschek, M. Schaechter, A. Tadmor, and members of the Hwa lab for suggestions and discussions; D. Hughes for the Sm mutant strains; and P.-h. Lee and B. Willumsen for the use of unpublished data. Supported by NIH grant RO1GM77298, NSF grant MCB0746581, and the NSF-supported Center for Theoretical Biological Physics (grant PHY0822283). M.S. was supported by a Natural Sciences and Engineering Research Council of Canada fellowship.

Symbiotic Bacterium Modifies Aphid Body Color

Tsutomu Tsuchida,[1]*† Ryuichi Koga,[2]† Mitsuyo Horikawa,[3] Tetsuto Tsunoda,[3] Takashi Maoka,[4] Shogo Matsumoto,[1] Jean-Christophe Simon,[5] Takema Fukatsu[2]*

Color variation within populations of the pea aphid influences relative susceptibility to predators and parasites. We have discovered that infection with a facultative endosymbiont of the genus *Rickettsiella* changes the insects' body color from red to green in natural populations. Approximately 8% of pea aphids collected in Western Europe carried the *Rickettsiella* infection. The infection increased amounts of blue-green polycyclic quinones, whereas it had less of an effect on yellow-red carotenoid pigments. The effect of the endosymbiont on body color is expected to influence prey-predator interactions, as well as interactions with other endosymbionts.

The world is full of colors, and many animals have color vision, recognizing their environment, habitat, food, enemies, rivals, and mates by visual cues. Body color is thus an ecologically important trait, often involved in species recognition, sexual selection, mimicry, aposematism, and crypsis (*1*, *2*). In the pea aphid *Acyrthosiphon pisum*, red and green color morphs are found in the same populations. Early work has shown that the aphid body color is genetically determined, with red being dominant over green (*3*). Ecological studies show that ladybird beetles tend to consume red aphids on green plants (*4*), and parasitoid wasps preferentially attack green aphids (*5*). The predation and parasitism pressures appear to maintain the color variation in natural aphid populations (*1*, *4*). An unexpected recent discovery showed that the aphid genome contains several genes for carotenoid synthesis not found in animal genomes. The genes are of fungal origin and appear to have been acquired in the evolutionary history of aphids via ancient lateral transfer. One of the genes is involved in synthesis of red color pigments, and the presence or absence of the gene is responsible for the red or green coloration of the aphids (*6*). Here, we report another factor affecting aphid color polymorphism: a previously unrecognized endosymbiont that modifies insect body color in natural populations.

While screening pea aphid strains from natural populations collected in France, we found several strains of green aphids producing red nymphs. As the nymphs grew, their body color changed from reddish to greenish, and the adults became

[1]Molecular Entomology Laboratory, RIKEN Advanced Science Institute, Wako 351-0198, Japan. [2]National Institute of Advanced Industrial Science and Technology (AIST), Tsukuba 305-8566, Japan. [3]Faculty of Pharmaceutical Sciences, Tokushima Bunri University, Tokushima 770-8514, Japan. [4]Research Institute for Production Development, Kyoto 606-0805, Japan. [5]Institut National de la Recherche Agronomique, UMR 1099 BiO3P, Institut National de la Recherche Agronomique (INRA)/Agrocampus Ouest/Université Rennes 1, BP 35327, 35653 Le Rheu Cedex, France.

*To whom correspondence should be addressed. E-mail: t-tsuchida@riken.jp (T.T.); t-fukatsu@aist.go.jp (T.F.)
†These authors contributed equally to this work.

Supporting Online Material for

Interdependence of Cell Growth and Gene Expression: Origins and Consequences

Matthew Scott, Carl W. Gunderson, Eduard M. Mateescu, Zhongge Zhang, Terence Hwa*

*To whom correspondence should be addressed. E-mail: hwa@ucsd.edu

This PDF file includes:

Materials and Methods
SOM Text
Figs. S1 to S6
Tables S1 to S7
References

Inter-dependence of Cell Growth and Gene Expression: Origins and Consequences

M. Scott, C. W. Gunderson, E. M. Mateescu, Z. Zhang and T. Hwa
Science (2010).

Supplemental Online Materials

Supporting Text

Materials and Methods

Strain construction

All the strains used in this study are derived from *Escherichia coli* K12 strain MG1655, apart from those strains derived from the XAC strain described below. Strain EQ2 that is deleted of both *lacI* and *lacZ* harbors a sp^r-*lacI^q*-*tetR* cassette (*1*) at the *attB* site, providing constitutive expression of *lacI* and *tetR*. This strain was used for all RNA and total protein extraction experiments reported in Fig. 1A and 2A. The XAC strain is the parental strain of the streptomycin mutants, UK285 (streptomycin resistant, SmR) and UK317 (streptomycin pseudoresistant, SmP)(*2, 3*), used to test the effects of impaired translation (Fig. 1B).

To make the strain that constitutively expresses *lacZ*, the *lacY* gene was first deleted using a recombineering protocol involving the *galK* positive selection and counterselection (*4*). The P$_{LtetO1}$ promoter (*1*) plus the downstream 5' untranslated region (UTR) containing the ribosome binding site was cloned into the *Sal*I and *BamH*I sites of pKD13 (*5*), yielding pKD13-P$_{LtetO1}$. The promoter plus the upstream Km^r gene (*Km^r*: P$_{LtetO1}$) in pKD13-P$_{LtetO1}$ was integrated into the chromosome to replace the *lacI* gene and the native *lac* promoter (including the 5' UTR of *lacZ*) using the method of Datsenko and Wanner (*5*). This strain was used as the donor to transfer the *lacZ* expression construct into EQ1 by P1 transduction. The resultant strain (EQ3), in which the *lacZ* gene is driven by P$_{LtetO1,}$ was used in all constitutive protein expression experiments (Figs. 2C, S4C and S5). The construction of the strain harboring a negatively autoregulated source of LacZ, EQ39 (Fig. S4BC), is detailed in Klumpp *et al.* (*6*).

To make strain EQ30 that was used in the overexpression experiment (Fig. 4), the *lacZ* structural gene was substituted for the *luc* gene in pZE32-*luc* (*1*), yielding pZE32-*lacZ*. The region containing P$_{LlacO1}$ and the 5-UTR in pZE32-*lacZ* was replaced by a σ^{54}-dependent P*u* promoter (*7*), yielding pZE32P*u-lacZ*, in which *lacZ* is solely driven by P*u*.

To constitutively activate the Pu promoter, the wild type *xylR* gene (*7*) was deleted of the first 675 bps from its 5' end, resulting in a shorter version of *xylR* (*dnxylR*) that encodes a constitutively active activator for Pu. The *dnxylR* gene was substituted for *gfp* in pZE12-*gfp*(*8*), yielding pZE12-*dnxylR*, in which *dnxylR* is driven by synthetic P$_{LlacO1}$ promoter. P$_{LlacO1}$ is derived from the P$_L$ promoter of phage lambda, with the binding sites for CI replaced by LacI. The P$_{Llac-O1}$-*dnxylR* construct from pZE12-*dnxylR* was cloned into the *Sac*I and *BamH*I sites of the integration plasmid pLDR10 and subsequently integrated to the *attB* site following the method of Diederich *et al.* (*9*). Expression of *dnxylR* was repressed by LacI^q, encoded by the plasmid pZS4Int1 (*1*). Therefore, the resultant strain (EQ30) contains 1) the plasmid pZE32Pu-*lacZ*, 2) the P$_{Llac-O1}$-*dnxylR* construct at the *attB* site, and 3) plasmid pZS4Int1. Thus, in the presence of IPTG, LacI is released from the P$_{LlacO1}$ promoter, activating expression of dn-*xylR*, which in turn activates expression of *lacZ*. EQ23 is a control strain that lacks the pZE32Pu-*lacZ* plasmid, and was used to show that the growth is not inhibited by the *galK* and *rhyB* deletions, nor by induction of the XylR protein.

Media and Growth Conditions

Minimal media were based upon Miller's M63 (*10*) (in 1 L): 13.6 g KH$_2$PO$_4$, 0.5 mg FeSO$_4$·7H$_2$O, 0.5 g MgSO$_4$·7H$_2$O and 10^{-4} % (w/v) Thiamine. Carbon (0.5% w/v) and nitrogen source (20 mM) were varied, as indicated in the figure and table captions. Rich defined media (RDM) is a MOPS buffered media supplemented with micronutrients, amino acids, and vitamins, as described by Neidhardt *et al.* (*11*). Aliquots of RDM were stored frozen at -20°C and thawed immediately before use. Seed cultures were grown in LB broth (Bio Basic) or RDM, and used to inoculate pre-cultures in appropriate growth media. After 8 to 10 hours of growth, precultures were pelleted, washed twice by centrifugation and resuspension in prewarmed media and used to inoculate experimental cultures (at a dilution of 100x-1000x). Cells were grown in 5 mL of culture media at 37°C in 20 mm test tubes, shaken in a water bath (New Brunswick Scientific) at 250 rpm. Growth rate was monitored by measuring OD$_{600}$ on a Genesys20 spectrophotometer (Thermo-Fisher) over time, with cell viability corroborated by plating. Optical density of the cultures was measured once or twice per doubling, depending on the growth rate. After at least 3 generations in unperturbed exponential growth, samples were collected to simultaneously assay RNA, protein, and/or LacZ content, as described below.

For treatments with ribosome-targeting drugs (chloramphenicol, tetracycline and kanamycin), antibiotics were added to the pre-culture at the same concentrations used in the experiments. The parent strain Xac, and the mutants derived from this strain, UK285 (SmR) and UK317 (SmP), are proline/arginine auxotrophs. All growth media for these strains contain 10mM proline and 2.5mM arginine, in addition to any other nitrogen sources listed.

RNA Extraction

1.8 mL of exponentially-growing culture was pelleted, fast-frozen in ethanol/dry ice and stored at -80°C. Pellets were resuspended in 100 μL TE buffer (10 mM Tris, 1 mM EDTA, pH 8.1) and 50 mg/mL lysozyme (Sigma, L6876), incubated at room temperature for 1 minute, and quantitatively transferred to a screw cap centrifuge tube containing 1 mL TRIzol reagent (Invitrogen, 15596-018) and 0.4 g 200 μm glass beads (Sigma, G1277). Samples were fully lysed using a FastPrep glass-bead homogenizer (MP

Biomedicals) set at maximum speed for 45 seconds, and RNA was extracted twice with chloroform and then precipitated with isopropanol according to the TRIzol protocol. RNA was pelleted via centrifugation, and washed with 70% ethanol. RNA pellets were briefly dried in a Speedvac concentrator to remove contaminating organic solvents. Purified RNA was resuspended in 100 µL of deionized water and the RNA concentration was determined by measuring the A_{260} using a NanoDrop 1000 spectrophotometer. The extraction efficiency was calibrated against RNA standards and a perchlorate extraction method (*12*).

Protein Extraction

200 µL of exponentially-growing culture was fast-frozen in ethanol/dry ice and stored at -80°C. Samples were thawed in 800 µL of deionized water and 0.015% (w/v) sodium deoxycholate (Sigma, D8566). Total protein content was measured with the Total Protein Kit (Sigma, TP0300) using a modified Lowry method, with bovine serum albumin (BSA) as the standard. Briefly, the test samples and BSA standards were individually diluted to 1 ml in enpendorf microtubes. 100 µl 0.15% Deoxycholate and 100 µl 72 % trichloroacetic acid (TCA) were added to each microtube. The samples were set at room temperature for 10 minutes, and then centrifuged at the maximum speed in a tabletop microcentrifuge machine for 10 minutes to pellet the total protein. The pellet was resuspended in 800 µl of 50% Lowry reagent (provided in kit) in water. After a 20 minute incubation, 200 µl Folin & Ciocalteu's Phenol reagent (provided in kit) was added to develop a blue color. The color was allowed to develop for 30 minutes, and the OD (wavelength of 750nm) of the samples were measured within 30 minutes. The BSA standard curve was used to quantify the total protein in each of the test samples.

To compute the RNA/protein ratio, the total RNA and total protein were assayed over a range of OD_{600}, and the slope of the resulting lines was used.

β-Galactoside Activity

400 µL samples were taken at least 4 times during exponential growth (typically at OD_{600} between 0.1 and 0.6). In instances where LacZ activity was normalized to total protein, an additional 200 µL sample was taken at each sample point for total protein determination, as described above. LacZ assay samples were immediately added to an equal volume of the freshly prepared Z-buffer (in 1 L: 8.52 g Na_2HPO_4, 5.5 g $NaH_2PO_4 \cdot H_2O$, 0.75 g KCl and 0.25 g $MgSO_4 \cdot 7H_2O$, pH adjusted to 7.0; with 0.004% (w/v) SDS and 40 mM β-mercaptoethanol) with 100 µl chloroform. Cells were disrupted by vortexing and stored at 4°C until all samples were collected. After all the samples were collected, they were briefly vortexed a second time. After 5-10 minutes at room temperature to settle the chloroform, the lysates were diluted (typically 1:20) into 50:50 mixture of Z-Buffer and media. 200 µL was then added to a 96-well plate (Sarstedt). Immediately prior to reading in GENiosPro (Tecan) plate reader, 40 µl of 4 mg/mL *ortho*-Nitrophenyl-β-galactoside (Sigma) in 0.1 M phosphate buffer (pH=7.0) was added to each well. The plate reader was set to read absorbance at a wavelength of 420 nm every minute for 60 to 120 minutes at 28°C.

The slope of the plot of OD_{420} vs. time (in minutes) for all replicates was used to calculate the β-galactosidase activity (Units/mL) in the original sample via the following conversion:

$$\beta\text{-galactosidase activity}\left(\text{U/mL}\right) = 2 \cdot 1000 \cdot \left[\frac{OD_{420}}{\min}\right] \cdot \left(\begin{array}{c} \text{fold} \\ \text{dilution} \end{array}\right) \cdot 2.66,$$

where the factor of 2 comes from the initial 1:2 dilution into Z-buffer/chloroform at the time of harvest. The factor of 2.66 converts the plate-reader data to the activity obtained using the original assay protocol by Miller (*10*), and is specific to the path-length through the sample (*i.e.* 240 μL in a 96-well plate). The slope of the plot of activity (U/mL) versus the sample OD_{600} yields the activity in Miller units (U/mL/OD_{600}). The enzyme activity was expressed in μg of β-galactosidase (1082 U/mL/ μg of β-galactosidase) calibrated with pure enzyme (Sigma), and normalized to total protein content.

Theoretical Analysis

In this section, we provide a derivation of the correlations [1] and [2] described in the main text, starting from a number of explicit postulates on *E. coli* growth physiology. Before starting, we remark that the existence of the correlations [1] and [2] (Fig. 1A and Fig. 2A) are empirical facts independent of the validity of the postulates and the derivation. Also, the consequences predicted from phenomenological approach presented in the main text (Eq. [3]-[6], supported by the data in Figs. 2 and 4) do not depend on these postulates and derivation. The purpose of the derivation is to illustrate a scenario for how these correlations could have arisen molecularly, and to give possible molecular interpretations for the phenomenological parameters (κ_t, κ_n, r_{max}). We also note the well-known fact that the linear correlation [1] does not hold for RNA/protein ratio (r) below 0.15, where r becomes independent of the growth rate (*13*). This work is clearly not applicable to the regime of very low r, corresponding e.g., to the conditions of very poor nutrients.

Conversion between RNA/protein ratio and the ribosomal fraction.
The correlations [1] and [2] in the text are expressed in terms of the RNA/protein ratio r which is readily quantified. However, derivation of these correlations is most naturally done in terms of the ribosomal mass fraction $\phi_R \equiv M_R / M$, where M_R is the total mass of the ribosomal proteins together with their affiliates (referred to below as the "extended ribosome"), including all the initiation factors, elongation factors, tRNA synthases, etc., and M is total mass of cellular proteins. A linear relation $\phi_R = \rho \cdot r$ has been used to relate these two quantities in the text. Here, we deduce the numerical value of the conversion factor ρ and discuss the assumptions underlying the linear relation between r and ϕ_R.

From the definitions of r and ϕ_R, the conversion factor is $\rho \equiv M_R / M_{RNA}$, where M_{RNA} is the total RNA mass. It can be written down as a product of 3 factors:

$$\rho \equiv \frac{M_{rRNA}}{M_{RNA}} \cdot \frac{M_{rp}}{M_{rRNA}} \cdot \frac{M_R}{M_{rp}},$$ where M_{rRNA} is the total mass of ribosomal RNA (rRNA), and

M_{rp} is the total mass of ribosomal proteins (r-proteins). The values of these three factors can be estimated as follows:

- The first factor is the mass fraction of rRNA among all RNA. Under nutrient conditions supporting moderate to fast growth (e.g., doubling time from 20

minutes to 2 h), rRNA/RNA mass ratio was found to be approximately 86% (*13, 14*). At slower rates of growth, tRNA/rRNA mass ratio increased leading to a decrease in rRNA/RNA (*13*). Similarly, under translational inhibition by chloramphenicol, rRNA was found to be somewhat unstable while tRNA accumulated (*15*). Nevertheless, the overall change in the steady-state rRNA/RNA mass ratio under translational inhibition by chloramphenicol was less than 10% (*16*). Both *severe* nutritional and translational limitation therefore led to a decrease in rRNA/RNA mass ratio. Over the range of growth rates shown in Figs. 1 and 2, however, the effect is expected to be small and we use $M_{rRNA} / M_{RNA} = 0.86$ for simplicity.

- The second factor is the mass ratio of r-proteins to rRNA, which comes straightforwardly from the known stoichiometry of the ribosome. The ribosomal proteins are composed of 7336 amino acids, and the rRNA is composed of 4566 nucleotides [Table 1, Ref. (*14*)]. Assuming that there are 5.6×10^{15} amino acid residues per μg of protein, and that the average molecular weight of an RNA nucleotide is 324 (*14*), yields $M_{rp} / M_{rRNA} = 0.53$.

  [Upon severe inhibition by chloramphenicol, the stoichiometry of the individual r-proteins is no longer conserved (*17*). However, the ratio of M_{rp} / M_{RNA} (the product of the first two factors) appears to be little affected in the range of chloramphenicol levels used in this study (0-12 μM). For example, comparing cells grown in medium with 12 μM and no chloramphenicol, the r-protein to total protein ratio (M_{rp} / M) changed by 2.94x (computed based on numbers given in Ref. (*17*)), while the total RNA to total protein ratio (M_{RNA} / M) changed by 2.74x in the present study. These numbers imply that the ratio M_{rp} / M_{RNA} changed by only 2.94/2.74 = 1.07x between 12μM and no chloramphenicol, assuming that the numbers are not strain dependent.]

- The third factor is the mass ratio of the r-proteins to the affiliated ribosomal proteins. This ratio was found to be $M_R / M_{rp} = 1.67$ for cells grown at 40 min doubling time [Table 4, Ref. (*14*)]. The dependence of this factor on growth conditions has not been characterized systematically to the best of our knowledge. It is however known that the mass fraction of several members of the "extended ribosome" increased with the growth rate similarly as the r-proteins for growth modulated by nutrient content of the medium (*18, 19*). Also, quite a number of the affiliated r-proteins are encoded by genes in the same operons as those encoding the r-proteins, suggesting co-expression of these proteins. This information motivated us to make the simplifying assumption that the mass of the extended ribosome scales with the ribosome mass by the same factor $M_R / M_{rp} = 1.67$ for all growth conditions. Further quantitative studies are clearly needed to better understand the dependence of this factor on different growth conditions.

Putting together the above factors for ρ, we have

$$\rho \equiv \frac{M_{rRNA}}{M_{RNA}} \cdot \frac{M_{rp}}{M_{rRNA}} \cdot \frac{M_R}{M_{rp}}$$

$$\approx \frac{0.86\,\mu g\,\text{rRNA}}{1\,\mu g\,\text{RNA}} \cdot \frac{0.53\,\mu g\,\text{r-protein}}{1\,\mu g\,\text{rRNA}} \cdot \frac{1.67\,\mu g\,\text{ extended ribosome}}{1\mu g\,\text{ r-protein}} \qquad \text{[S1]}$$

$$= 0.76\,\mu g\,\text{protein}/\mu g\,\text{RNA}$$

which is one of the basic parameters used in the main text.

General formulation of protein synthesis and ribosome allocation.
We shall start with the postulate that all ribosomes are active and elongate at a fixed rate k *(13)*. Consider three classes of proteins in the proteome, P, Q, R, of masses M_P, M_Q, and M_R. Let the fraction of ribosomes devoted to synthesizing each class be f_P, f_Q, and f_R, respectively, with $f_P + f_Q + f_R = 1$. Molecular control on the relative synthesis of the different fractions resides in these f s as will be discussed below. Under the assumption that protein turnover is negligible *(20)*, each class of proteins accumulate according to the equations

$$\frac{d}{dt} M_P = f_P \cdot k \cdot N_R, \qquad \text{[S2]}$$

$$\frac{d}{dt} M_Q = f_Q \cdot k \cdot N_R, \qquad \text{[S3]}$$

$$\frac{d}{dt} M_R = f_R \cdot k \cdot N_R, \qquad \text{[S4]}$$

where N_R is the total number of actively translating ribosomes (which, by postulate, is the total number of ribosomes). The total protein mass $M \equiv M_P + M_Q + M_R$ accumulates according to

$$\frac{d}{dt} M = k \cdot N_R. \qquad \text{[S5]}$$

Defining the R-class of the proteome to be the r-proteins and their affiliates (as described above), and assuming that all ribosomes are actively engaged in translation, then $M_R = m_R \cdot N_R$, where m_R is the protein mass of an "extended ribosome" (i.e., the mass of r-proteins m_{rp} together with the mass of affiliated proteins per ribosome), and the above equations yield the exponential steady state, $M_R(t) = M_R(0) \cdot e^{\lambda t}$, $M_P(t) = M_P(0) \cdot e^{\lambda t}$, and $M_Q(t) = M_Q(0) \cdot e^{\lambda t}$, with

$$\lambda M_P = f_P \cdot \lambda M, \qquad \text{[S6]}$$

$$\lambda M_Q = f_Q \cdot \lambda M, \qquad \text{[S7]}$$

$$\lambda = f_R \cdot k / m_R, \qquad \text{[S8]}$$

$$\lambda M = k \cdot M_R / m_R. \qquad \text{[S9]}$$

Note that Eqs. [S6]-[S8] describe an equality between the proteome fraction (M_X / M) of class X proteins and the fraction of ribosome (f_X) devoted to the synthesis of X.

Correlation [1] and the control of ribosome synthesis.

In terms of the ribosomal mass fraction $\phi_R \equiv M_R / M$, Eq. [S9] can be written as

$$\phi_R = \frac{\lambda}{k / m_R},\qquad\qquad [S10]$$

which together with the conversion $\phi_R = \rho \cdot r$, reproduces the correlation [1] with $r_0 = 0$. The case of a non-zero vertical offset ($r_0 > 0$ in [1]) results from the fact that not all ribosomes are actively translating and will be addressed in detail elsewhere. Here we discuss other aspects of Eq. [1].

Comparison of Eq. [S10] with Eq. [1] of the main text yields

$$\kappa_t = \rho \cdot k / m_R.\qquad\qquad [S11]$$

This relation allows us to estimate the translational elongation rate k from the observed value of the "translational capacity" κ_t from Table S1. We have

$$k = \frac{\kappa_t}{\rho / m_R} = \frac{\kappa_t \cdot m_{rp}}{\dfrac{M_{rRNA}}{M_{RNA}} \cdot \dfrac{M_{rp}}{M_{rRNA}}}\qquad\qquad [S12]$$

$$\approx \frac{(4.5\,\mu g\ \text{protein}/\mu g\ \text{RNA/h}) \cdot (7336\,\text{a.a./r-protein})}{0.86 \times (0.53\,\mu g\ \text{r-protein}/1\,\mu g\ \text{rRNA})} = 20.1\ \text{aa/sec}$$

close to the maximal ribosomal speed estimated (*13*). Note that this estimate is independent of the (somewhat uncertain) value of the mass of the affiliated r-proteins.

The key assumption made in the derivation of Eq. [S10] is the growth-rate independence of the translational elongation rate, k. Determination of the elongation rate in different growth media in the 1970s (*21*) suggested a decrease in k for slow growth. However, as criticized already by Maaløe (*13*), the method of Ref. (*21*), based on analyzing the incorporation of radioactively labeled amino acids, is *indirect* due to the variable size of the unlabeled, pre-pulse cytoplasmic amino acid pool, which is generally growth-rate (and possibly medium) dependent (*13*). The other popular method of determining peptide elongation rate, by following the first appearance of β-galactosidase upon induction, is affected by delay due to a number of processes including transcription and translation initiation, and protein maturation, each of which may be growth-rate dependent. Thus a direct method of measuring peptide elongation *in vivo* is needed before this issue can be resolved.

Within our model (Eq. [S2]-[S5] or Eq. [S6]-[S9]), the fraction of ribosomes synthesizing ribosomal proteins, f_R, plays a key role in the control of ribosome synthesis. In fact, a comparison of Eq. [S8] and [S10] yields the result $\phi_R = f_R$, i.e., the ribosomal fraction of the proteome is directly set by f_R. Also, Eq. [S8] shows that f_R directly sets the growth rate. Molecularly, the synthesis of ribosomal proteins is indirectly controlled by the transcription of ribosomal RNA[1], since ribosomal protein monomers can autoregulate their own translation to ensure that r-protein synthesis is commensurate with the rRNA synthesis (*22*). The latter is in turn repressed by the alarmone ppGpp (*23*), which is synthesized in response to uncharged tRNA (*24*). The alarmone ppGpp thus provides a link between nutrient supplies (which ultimately determines the amino acid supply for

---

[1] The existence of an analogous mechanism(s) for controlling the synthesis of the cohort of associated ribosomal proteins is presently not known.

tRNA charging) and ribosome synthesis f_R, with the latter ultimately determining the growth rate through Eq. [S8].

Despite this well-established molecular link, the growth-rate dependence of the ribosomal fraction, as characterized by Eq. [S10], should not be viewed as a consequence of specific regulatory mechanism such as the one mediated by ppGpp. Instead, we expect Eq. [S10] to be satisfied (up to an offset) for all exponentially growing cultures if the four conditions listed above are met. In fact, identical dependence of the RNA/protein ratio on growth rate was observed for relaxed strains, in which the synthesis of ppGpp was disabled (*25*). This may be due to an unknown regulatory pathway on ribosome synthesis, or it could be due to a set of built-in mechanisms that enforce the 4 conditions although not explicitly controlling ribosome synthesis.

The three-component partition of the proteome.
In our analysis so far, we have not discussed the non-ribosomal sectors of the proteome, referred to as P and Q. The existence of a number of such sectors does not affect the above analysis, as long as there is at least one non-ribosomal sector whose proteome fraction could be adjusted to accommodate the increase/decrease in the ribosomal fraction at different growth rates. (Such a sector must exist since the proteome fractions must sum to 1.) Based on the data in Fig. 2A (in particular the existence of a maximal ribosomal fraction at $\phi_R^{max} \approx 55\%$), we suggest a minimal 3-component model of the proteome in terms of the growth-rate dependencies, with a growth-rate independent sector (Q) occupying a mass fraction

$$\phi_Q = 1 - \phi_R^{max}, \qquad\qquad [S13]$$

and a flexible component (P) which "yields" to the need to establish a variable ribosomal fraction ϕ_R at different growth rates, with

$$\phi_P = \phi_R^{max} - \phi_R. \qquad\qquad [S14]$$

Beyond the fact that $\phi_R^{max} = 0.55 < 1$, the three-component model can be motivated in the following way: if only two partitions (R and NOT R) are considered, then under optimal growth conditions with all building blocks of biosynthesis provided (as e.g., in rich medium), the only task needed for cell growth is for the ribosomes to synthesize themselves. At an elongation rate of 20aa/sec, it takes around 6 minutes for a ribosome to assimilate the 7336 amino acid residues contained in a ribosome. Even if one expands the definition of the ribosome to include the cohort of other translational proteins (elongation factors, tRNA synthases, etc) that expand the size of a ribosome by ~67% (see the paragraph preceding Eq. [S1]), this only changes the 6 minutes to 10 minutes, a result that is twice the fastest rate of cell doubling observed in E. coli. The 3-partition model essentially imposes a fixed "entitlement" to the workload of the ribosomes – it requires that ~50% of the proteome (the Q-class non-ribosomal proteins) be reproduced in addition to the reproduction of the ribosomes themselves – no matter what the growth conditions are. This 50% extra work load for the ribosomes reduces the minimal time for reproduction from 10-min to 20-min, in line with the observed maximal growth rate. Note that there is no parameter fitting to obtain this estimate: $\phi_R^{max} \sim 55\%$ is a hard number suggested by the correlation in Fig.2A (Eq. [2] in the main text). Together with the elongation rate of the ribosomes, it automatically gives the maximal growth rate of the cell. (Formally, it is given by the maximal growth rate λ_c of the Michaelis-Menton relation for cell growth, Eq.[5]). Within the 3-partition model, the value of ϕ_R^{max} also

determines two other independent quantities: (i) the mass fraction of over-expressed proteins at which growth ceases, which is the horizontal intercept of the lines shown in Fig.4B (see Eq. [S31]), and (ii) the growth rate at which constitutively expressed proteins drops to zero expression (see Fig. S5 and Eq. [S26]). Thus, this 3-partition model, forced upon us by the observation that $\phi_R^{\max}$ is well under 100%, explains simultaneously three independent and very important physiological quantities in quantitative terms without any adjustable parameters. We regard the result $\phi_R^{\max} \sim 55\%$ (and hence the 3-partition model it suggests) as perhaps the most surprising and significant finding of this study.

Proteome partition and gene regulation.
From Eqs. [S6] and [S7], we have $\phi_P = f_P$ and $\phi_Q = f_Q$. Thus, the abundances of the P and Q sectors are set respectively by f_P and f_Q, the fractions of the ribosome devoted to synthesizing proteins belonging to the P- and Q- sectors. Molecularly, these fs are controlled by two factors, the abundance of the mRNAs encoding the respective proteins, and the translational initiation rate of each mRNA transcript[2]. The latter is encoded by the quality of the ribosome binding sequence and further modulated by the accessibility of the translational initiation region of the transcript (*26*).

In the above, we already mentioned that the inhibition of ribosomal proteins on the translation of their own mRNA, a way of controlling translational initiation by affecting the accessibility of the translational initiation region, is ultimately the way by which f_R is controlled. We have also shown data (Fig. S4C) supporting the hypothesis that negative autoregulation is a way for ϕ_Q to remain growth-rate independent. Under negative

regulation, transcription of a gene (hence the abundance of the mRNA) would be automatically adjusted until a fixed concentration of proteins [set by the feedback circuit – see Refs. (*6*) and (*27*)] is reached. A fixed (i.e., growth-rate independent) protein concentration is translated to a fixed proteome fraction since the ratio of the biomass to cell volume is growth-rate independent [see Ref. (*28*). Note, however, that this would no longer be the case if osmolarity of the medium is varied; see Ref. (*29*)].

Along this line, the necessary growth-dependent modulation in the translation of the proteins in the P-sector, which must be adjusted to complement growth-rate dependent changes in the R- sectors, could be accomplished if there are no specific regulatory mechanisms to compensate for the abundance or accessibility of these transcripts at different growth rates. Unregulated or constitutively expressed proteins would therefore naturally belong to this sector, as was demonstrated explicitly in Fig. S5. The final result of the regulatory process is somewhat counter intuitive: The expressions of unregulated genes are growth-rate dependent while the expressions of (negatively auto-) regulated genes are growth-rate independent. This result is elaborated in Ref. (*6*).

Note that direct examinations of the proteome partition model using mRNA-based high-throughput methods such as the DNA microarray (*30*) are complicated by the growth-rate dependence of the relation between mRNA and protein abundances (*6*). For example, the growth-rate independence of the protein abundance of negatively autoregulated genes requires growth-rate dependent changes in their mRNA abundances.

It is important to keep in mind that this 3-component view of the proteome is the minimal one necessary to accommodate the data in Fig. 1A and 2A, obtained for media

---

[2] Here we have assumed that premature termination of translation does not play a dominant role.

with generally good nutrient conditions and under no specific stresses. The situation may well become more complex (e.g., requiring the introduction of additional protein classes) under conditions that elicit specific programmed responses, such as anaerobic growth or growth in conditions of high acidity or high osmolarity. Also, membership in any one class (R,P or Q) need not be exclusive for a given protein. It is possible, for example, that a non-ribosomal protein maintains a nonzero-fraction of the proteome at high chloramphenicol concentrations, but nonetheless increases with increasing growth rate as the antibiotic level decreases – the off-set at zero growth would be classified as belonging to Q, while the growth-rate dependent fraction would be classified as belonging to P.

Nutrient influx, metabolic bottleneck, and the correlation [2].
Empirically, the growth rate of a culture is set by the quality of nutrients in batch culture growth. Typically, the concentrations of nutrients used well exceed saturation (so that an exponentially growing culture can be sustained for an appreciable period of time). Thus given the nutrient composition, growth limitation is internal, e.g., due to limitations in the abundance or activity of enzymes belonging to a growth-limiting metabolic pathway.

For simplicity, consider a case where the growth bottleneck resides completely in one enzyme, E. [Generalization to the more realistic case where the bottleneck is distributed throughout a pathway is straightforward using Metabolic Control Analysis (*31*).] Let the mass of the bottleneck enzymes be M_E. Then the growth rate λ is completely dictated by the flux J of the growth-limiting nutrient processed by E,

$$\lambda M = c \cdot J = c \cdot k_E \cdot M_E,$$ [S15]

where the proportionality constant c reflects the nature of the growth limiting nutrient, and k_E is the kinetic constant of the enzyme E [3]. Assuming that the bottleneck enzyme belongs to the P-sector of the proteome, then the mass fraction of E is

$$\phi_E \equiv M_E / M = \alpha_E \cdot \phi_P$$ [S16]

where the proportionality factor α_E describes the fraction of P that is E, and is set by the expression level of the enzyme. Eqs. [S15] and [S16] yield

$$\lambda = c \cdot \alpha_E \cdot k_E \cdot \phi_P,$$ [S17]

a linear relation between the P-fraction and growth rate. This is a derivation of Eq. [4] of the main text, from which we can identify the nutritional capacity κ_n as

$$\kappa_n = c \cdot \alpha_E \cdot k_E \cdot \rho.$$ [S18]

Thus, our model predicts this nutritional capacity to depend on the expression and activity of the bottleneck enzyme, as one would intuitively expect. Furthermore, the collection of parameters that define the nutrient capacity will depend upon the composition of the growth medium and the particular growth-limiting pathway. Consequently, the nutrient capacity will change with different carbon and nitrogen sources, but in such a way that the growth rate and the nutrient capacity are positively correlated (Fig. S3A). By combining with Eq. [S14], we obtain,

---

[3] For saturating nutrients, k_E would just be the maximal catalytic rate of the enzyme E. The same analysis can be extended to nutrients which are not saturating but nevertheless hold constant throughout growth. An example may be the oxygen level in a continuous culture kept at in partially aerated state. In the latter case, we would have $k_E = k_E^{cat} \cdot [n]/(K_E + [n])$, where $[n]$ is the level of the growth-limiting nutrient.

$$\phi_{\text{R}} = \phi_{\text{R}}^{\max} - \phi_{\text{P}} = \phi_{\text{R}}^{\max} - \lambda / (c \cdot \alpha_{\text{E}} \cdot k_{\text{E}}), \tag{S19}$$

which is a statement of Eq. [2].

It should be emphasized that in this derivation of correlation [2] (Eq.[S19]) does not depend in any special way on the use of antibiotic. It simply expresses a relation between growth rate and the ribosomal fraction under the condition that the growth-limiting nutrient (and hence the bottleneck enzyme) is fixed and also $\phi_{\text{R}}^{\max}$ is fixed. In this context, applying antibiotics is a particular way to change the growth rate without changing these two conditions, so that correlation [2] may be revealed. We take Eq. [S17] as the more fundamental relation that relates nutrient influx (via biosynthesis or transport) to growth, and Eq. [2] as merely a revelation of this fundamental relation under appropriate conditions.

The key assumption that the relation [S17] depends on is the membership of the bottleneck enzyme(s) in the P-sector. Given the 3-component partition of the proteome, there is little choice for the placement of the metabolic bottleneck: The assignment of the bottleneck in the P-sector recovers Eq. [2] as shown above, while the assignment of the bottleneck in the Q- or R- sector both yields nonsense. Physiologically, this assumption may be rationalized by the following two propositions:

    (i) catabolic enzymes belong to the P-sector,
    (ii) bottleneck enzymes reside in catabolism.

The first proposition is rooted in the regulatory structure of the metabolic network. Catabolic pathways are mostly regulated by positive feedback (for example, *lacZY* for lactose utilization, *glpFK* for glycerol utilization, *araBAD* for arabinose utilization, etc.), such that a pathway is only expressed when the particular nutrient is available and needed (*32*). Under the condition of saturating nutrients then, the catabolic enzymes should be maximally expressed once induced. As such, they may be regarded as unregulated and hence belonging to the P-sector. Proteins in the P-sector contrast starkly with the expression of negatively autoregulated genes (Fig. S4C). The positive regulation of catabolic enzymes may be interpreted as a strategy by the cell to conserve the proteome for only those proteins that are needed in the current growth condition.

The second proposition may be viewed as a consequence of the "bow-tie" organization of the metabolic network (*32-34*). Whereas the catabolic pathways responsible for turning specific nutrients into a small number of central precursor metabolites may be expressed as needed, the anabolic pathways responsible for turning the precursors into the biosynthetic building blocks (e.g., amino acids and nucleotides) are needed for most nutrients. Placement of the metabolic bottleneck in the anabolic sector is likely to burden the cell with a significant disadvantage; specifically, the fastest growth rate achievable would be that given by the bottleneck.

The integrated growth theory

Within the above framework, a rational guideline for the partitioning of the proteome may be formulated as follows: Assign to the Q-sector a fraction of the proteome which would adequately supply the flux of building blocks for the fastest possible growth rate (such that the Q-sector never presents as a growth bottleneck); fill the P-sector with the catabolic enzymes needed for a specific nutrient. In this way, the growth rate corresponding to a specific nutrient is established as a balance between the need for a large R-sector to maintain fast growth and the need for a large P-sector to supply the large nutrient demanded by fast growth. This balance is illustrated graphically in Fig. 3C.

Mathematically, the constraints are captured by the following three equations which form the foundation of this growth theory:

$$\phi_R = \rho \cdot \lambda / \kappa_t + \phi_0, \qquad\qquad [S20]$$

$$\phi_P = \rho \cdot \lambda / \kappa_n, \qquad\qquad [S21]$$

$$\phi_P + \phi_R = \phi_R^{max}. \qquad\qquad [S22]$$

These are analogous to Ohm's law applied to two resistors in series, with growth rate λ playing the role of current, the capacities (κ_t, κ_n) playing the role of the conductance of each resistor, and the protein fractions (ϕ_R,ϕ_P) playing the role of the voltage drop across each resistor (see Fig. S6).

In this theory, the growth rate λ and the ribosome partition (ϕ_R, ϕ_P) are dictated by the "collective variables" κ_t, κ_n, and ϕ_R^{max}, whose molecular origins have been suggested above, within the confines of the stated assumptions. Their dependences can be obtained by solving Eqs. [S20],[S21], and [S22], with the solution:

$$\lambda\left(\kappa_t, \kappa_n, \phi_R^{max}\right) = \frac{\phi_R^{max} - \phi_0}{\rho} \cdot \frac{\kappa_t \kappa_n}{\kappa_t + \kappa_n}, \qquad\qquad [S23]$$

$$\phi_R\left(\kappa_t, \kappa_n, \phi_R^{max}\right) = \left(\phi_R^{max} - \phi_0\right) \cdot \frac{\kappa_n}{\kappa_t + \kappa_n} + \phi_0, \qquad\qquad [S24]$$

$$\phi_P\left(\kappa_t, \kappa_n, \phi_R^{max}\right) = \left(\phi_R^{max} - \phi_0\right) \cdot \frac{\kappa_t}{\kappa_t + \kappa_n}. \qquad\qquad [S25]$$

Eq. [S23] is just the Michaelis-Menten form of growth described in the main text (Eq. [5]). While it is identical in form to the Monod equation describing growth inhibition upon substrate *availability* (*35*), notice that Eq. [S23] (Eq. [5]) describes growth inhibition upon substrate *quality* through the parameter κ_n. The theory predicts that if the growth rate is varied by keeping κ_t fixed, then Eq. [1] is obtained, while if the growth rate is varied by keeping κ_n and ϕ_R^{max} fixed, then Eq. [2] is obtained. Furthermore, combining Eq. [S23] and [S25], the theory predicts a linear decrease in ϕ_P,

$$\phi_P = \frac{\rho}{\kappa_t}\left(\lambda_c - \lambda\right), \qquad\qquad [S26]$$

where $\lambda_c = \kappa_t\left(\phi_R^{max} - \phi_0\right)/\rho$ (see Fig. S5).

There are of course many other ways of changing the growth rate, by which two or even all three of the collective variables may be affected. An example of this is altering the growth rate by changing temperature, which would change not only the ribosome elongation rate (hence κ_t), but also the catalytic rate of the bottleneck enzymes (hence κ_n), and perhaps even ϕ_R^{max} via changing the regulator-DNA binding affinities of the autoregulatory circuits hypothesized to maintain the Q-sector. Altering growth rate by changing medium osmolarity may produce global perturbations due to changes in the biomass to cytoplasmic water ratio (*28*). When multiple parameters are affected, the forms of correlations [1] and [2] may not be maintained even if the core elements (Eqs. [S20], [S21], and [S22]) remain valid.

Growth defect due to unnecessary protein expression

The growth theory developed above can be used to predict the effect of unnecessary protein expression on growth. Let the mass fraction of the unnecessary protein be ϕ_U. For proteins that do not exert specific toxic effect on the host, we may model the effect of unnecessary expression by adding ϕ_U to the proteome partition, implemented by changing Eq. [S22] to

$$\phi_P + \phi_R + \phi_U = \phi_R^{max}, \qquad [S27]$$

assuming that the expression of unnecessary proteins do not affect the core sector Q (hence not affecting $\phi_R^{max} = 1 - \phi_Q$). To see how the partition between the R- and P- sector adjust to a *fixed* ϕ_U imposed on the new system, we simultaneously solve Eqs. [1], [3], and [S27] to obtain

$$\lambda\left(\kappa_t, \kappa_n, \phi_R^{max}; \phi_U\right) = \frac{\phi_R^{max} - \phi_0 - \phi_U}{\rho} \frac{\kappa_t \kappa_n}{\kappa_t + \kappa_n}, \qquad [S28]$$

$$\phi_R\left(\kappa_t, \kappa_n, \phi_R^{max}; \phi_U\right) = \rho r = \left(\phi_R^{max} - \phi_0 - \phi_U\right) \frac{\kappa_n}{\kappa_t + \kappa_n} + \phi_0, \qquad [S29]$$

$$\phi_P\left(\kappa_t, \kappa_n, \phi_R^{max}; \phi_U\right) = \left(\phi_R^{max} - \phi_0 - \phi_U\right) \frac{\kappa_t}{\kappa_t + \kappa_n}. \qquad [S30]$$

Compared to the solutions discussed in the main text, unnecessary protein expression is seen as effectively reducing ϕ_R^{max}. Eq. [S28] can be written more succinctly as

$$\lambda\left(\kappa_t, \kappa_n, \phi_R^{max}; \phi_{UE}\right) = \lambda\left(\kappa_t, \kappa_n, \phi_R^{max}; \phi_{UE} = 0\right) \cdot \left(1 - \frac{\phi_{UE}}{\phi_R^{max} - \phi_0}\right), \qquad [S31]$$

which is the same as Eq. [6] of the main text.

Supplementary Figures

Figure S1
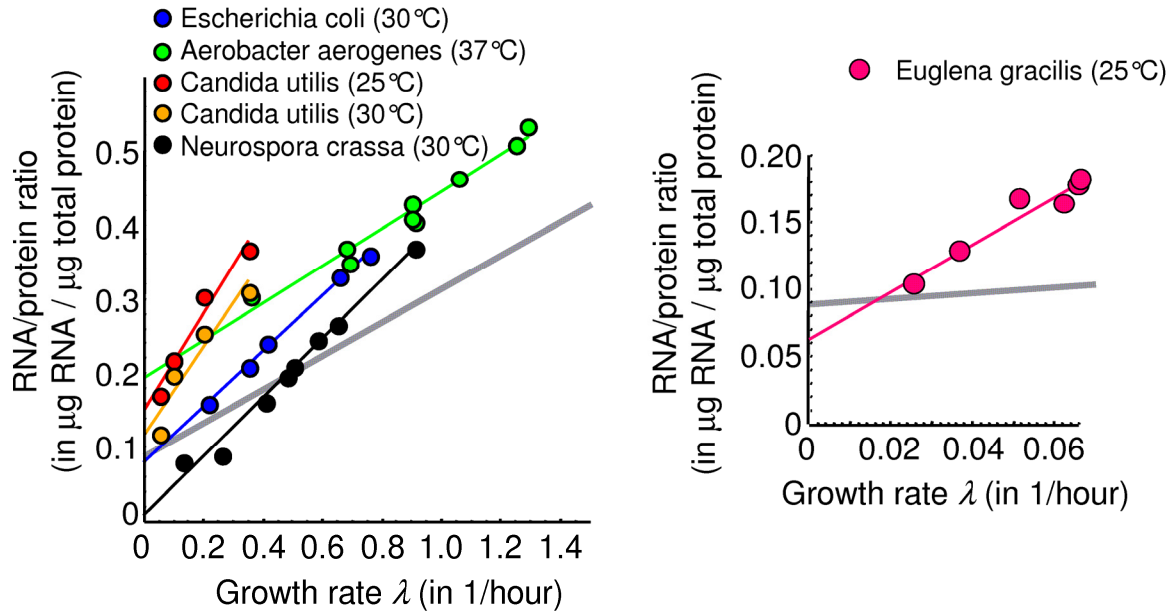
Fig. S1: Linear correlation between RNA/protein ratio and growth rate in various microbes. The linear relation between the RNA/protein ratio and the growth rate is evident in a number of bacteria studied, and in exponentially growing unicellular eukaryotes. *Left*: *Escherichia coli* (blue, 30°C; Ref. (*36*)), *Aerobacter aerogenes* (green, 37°C; Ref. (*37*)), *Candida utilis* (red, 25°C and orange, 30°C; Ref. (*38*)), *Neurospora crassa* (black, 30°C; Ref. (*39*)). *Right*: *Euglena gracilis* (magenta, 25°C; Ref. (*40*)).

For comparison, the grey line corresponds to the solid line drawn in Fig. 1A for various *E. coli* strains grown at 37°C.
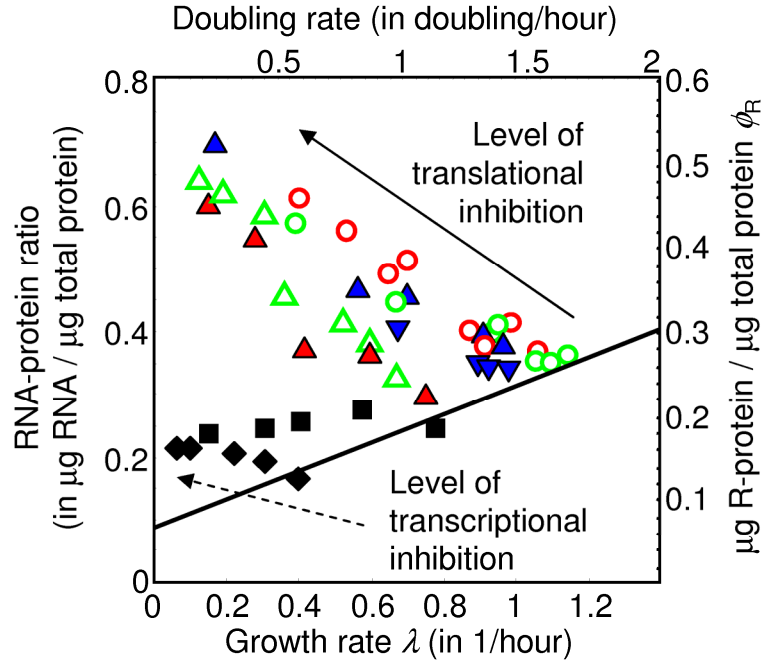
Fig. S2: Effect of translation inhibition on RNA/protein ratio. The linear increase in the RNA/protein ratio for translational inhibition using sub-lethal doses of chloramphenicol described in the main text is likewise observed for different methods of translational inhibition and in different strains: our K12 strain EQ2 with tetracycline or neomycin (filled triangles); B strain with inducible translation initiation factor 2 (IF2) (open red circles; Ref. (*41*)) and initiation factor 3 (IF3)(open green circles; Ref. (*42*)), where translational inhibition is affected by decreasing the level of an inducer. B/r strain at 30°C using chloramphenicol (open triangles; Ref. (*16*)).

Rifampicin (0-12 mM) is an inhibitor of transcription; the effect on the RNA/protein ratio for sub-inhibitory levels of rifampicin is strikingly different from the effect observed in translational inhibition (squares and diamonds).

Solid line as in Fig. 1A of the main text. Data are given in Table S5.
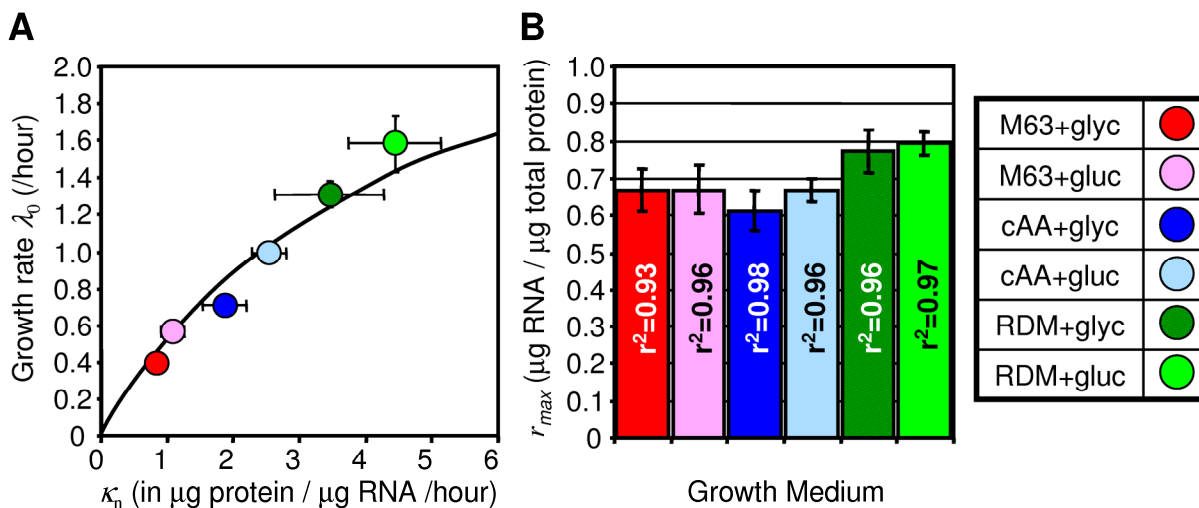
Fig. S3: A, The nutritional capacity κ_n (listed in Table S4) is positively correlated with the growth rate λ_0 of cells in the corresponding medium without antibiotics. This correlation is quantitatively accounted for by the Michaelis-Menten relationship (the black curve) derived in Eq. [5] of the text,

$$\lambda_0 = \lambda_c \frac{\kappa_n}{\kappa_n + \kappa_t},$$

with $\lambda_c = \kappa_t (r_{max} - r_0) \approx 2.85 /h$ from Table S4 and $\kappa_t = 4.5$ µg protein / µg RNA /h from Table S1. Error bars represent standard deviation over repeated measurements (for λ_0), and error in weighted-least squares linear regression (for κ_n). **B,** Linearity coefficient for each of the straight-line fits shown in Fig. 2A of the main text, along with the vertical intercept, r_{max}. Error bars denote the error associated with a weighted-least squares linear fit to the data (Table S4).

Fig. S4: **Growth-rate dependence of proteome components. A,** In our model, proteins in the proteome are grouped into three classes according to their growth-rate dependence as described in the main text and Fig. 3A: a R-class comprising of the ribosomal proteins and other proteins affiliated with 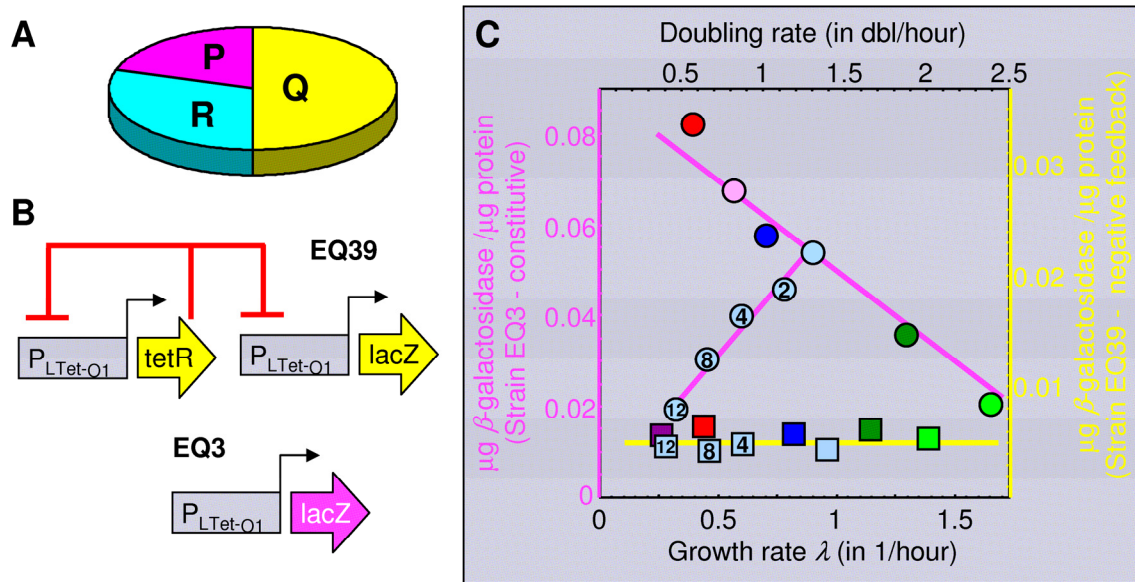translation, with the growth-rate dependences found in Fig. 1A and 2A according to different modes of growth limitation; a growth-rate independent Q-class; and a P-sector containing the remainder, including constitutively expressed proteins. **B,** Strain EQ39 expresses β-galactosidase (LacZ) under the control of a synthetic Tet promoter where the Tet repressor (TetR) is put under negative autoregulation (*6*). Strain EQ3 (Fig. 2C) expresses β-galactosidase (LacZ) under the control of the same Tet promoter, which is regarded as a constitutive promoter in the absence of the regulator TetR. **C,** Growth-rate independence of protein expression may be maintained molecularly through negative autoregulation: The expression of LacZ reporter under the control of a negatively autoregulated TetR repressor in strain EQ39 (*6*) is seen to be independent of the growth rate for either nutrient-limited or Cm-inhibited growth [squares, right axis]; see Table S6 for data. For comparison, constitutive LacZ expression in the isogenic *tetR*-null strain EQ3 exhibits strong growth-rate dependences (circles, left axis); data reproduced from Fig. 2C. The same color scheme as Fig. 2 is used to indicate the different nutrients in the medium [purple square corresponds to glycine medium described in Table S6]; the numbers in the symbols indicate the chloramphenicol dose in μM. For EQ39, 20ng/ml of the inducer chlortetracycline (cTc) was added to the growth medium in order to obtain enough LacZ expression for reliable measurement; see Ref. (*6*).
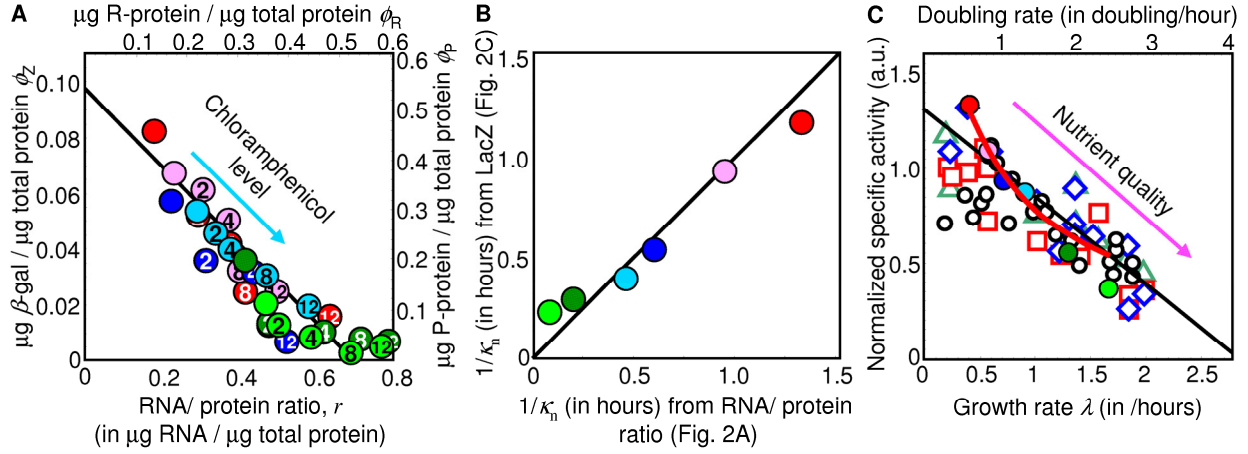
Fig. S5: Relation between gene expression and growth. A, *E. coli* strain EQ3 expressing *lacZ* driven by a constitutive P_{LtetO1} promoter on the chromosome (see SOM Methods) was grown in medium with various nutrients (same symbols as Fig. 2). Mass fraction of β-galactosidase (ϕ_Z) is plotted against the corresponding RNA/protein ratio from Fig. 2A. The line indicates the constraint $\phi_R + \phi_P = \phi_R^{max}$, using $\phi_R^{max} = 0.55$ (Table S4), with the scaling $\phi_P = \phi_Z/0.18$ (right vertical axis). **B,** The values of κ_n deduced from Fig. 2A correlated well with the κ_n values obtained from Fig. 2C (r^2=0.91). **C,** Negative correlation of constitutive gene expression with the growth rate for growth modulated by nutrient sources. Shown are specific activities of β-galactosidase (filled colored circles are zero chloramphenicol data from Fig. 2C), *o*-transcarbamylase (open green triangle; Refs. (*13, 43*)), β-galactosidase (open blue diamond; Refs. (*13, 43*)), and enzymes from the *trp*-operon (open red squares; Refs. (*13, 43*)). Also shown is the expression of L1-type constitutive mutants of the *lac* operon (open black circles; Ref. (*44*)). To compare among strains and enzymes, the specific activity was normalized to 1 at 1 dbl/h. Solid black line shows the prediction according to Eqs. [1] and [3],

$$\phi_P = \frac{\rho}{\kappa_t}\left(\lambda_c - \lambda\right),$$

see Eq. [S26] of SOM. Shown for comparison is the prediction of Ref. (*6*) (red curve) based on growth rate dependences of various measured cellular parameters.

$$\phi_R + \phi_P = 1 - \phi_Q \equiv \phi_R^{max}$$

$$\Rightarrow \lambda = \kappa_n \cdot \phi_P / \rho$$
Nutrient influx

$$\Rightarrow \lambda = \kappa_t \cdot (\phi_R - \phi_0) / \rho$$
Protein synthesis
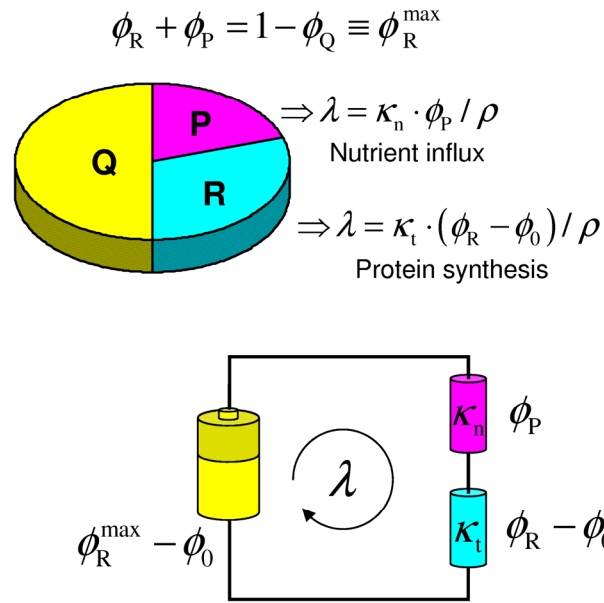
Fig. S6: Ohm's law analogy for resource allocation and growth control. The growth theory comprising of Eqs. [1], [3], and [4] is identical to the mathematical description of electric current flow in a circuit consisting of a pair of resistors, connected in series to a battery with voltage $(\phi_R^{max} - \phi_0)$. In this analogy, the growth rate λ is the current through the resistors. The voltage drop across each resistor corresponds to the mass fractions ϕ_P and $(\phi_R - \phi_0)$. The two equations $\lambda = \kappa_n \phi_P / \rho$ and $\lambda = \kappa_t (\phi_R - \phi_0)/\rho$ are seen as Ohm's law describing the voltage-current relation for each resistor, with conductance κ_n / ρ (magenta) and κ_t / ρ (cyan). The nutrient- and translation- modes of growth limitation correspond to changing the conductance of one of the resistors, while the expression of unnecessary protein is analogous to changing the applied voltage by decreasing ϕ_R^{max}. The Michaelis-Menten relation for growth (Eq. [5]), written alternatively as,

$$\lambda = \frac{(\phi_R^{max} - \phi_0)}{\rho} \frac{\kappa_n \kappa_t}{\kappa_n + \kappa_t},$$

corresponds to the current-voltage relation for the two resistors in series.

Supplementary Tables

Table S1 - Experimental data from Fig. 1A

From Fig. 1A – using a linear-regression fit to all three data sets: $\kappa_t = 4.5\pm0.2$ µg total protein/µg RNA/h; $r_0 = 0.087\pm0.009$ µg RNA/µg total protein. Error is displayed as ± the error associated with the linear fit. The R-protein fraction is related to the RNA/protein ratio by the conversion: $\phi_R = \rho \cdot r$, with $\rho = 0.76\,\mu$g protein / μg RNA (see Eq. [S1]).

Medium[a]	Growth rate λ (/h)[b]	RNA/Protein (µg/µg)	Source	Symbol
M63+glyc	0.40±0.03 (2)	0.177±0.006 (2)	This study	
M63+gluc	0.57±0.02 (5)	0.230±0.014 (2)		
cAA+glyc	0.71±0.03 (4)	0.224±0.029 (3)		
cAA+gluc	1.00±0.05 (5)	0.287±0.009 (3)		
RDM+glyc	1.31±0.07 (3)	0.414±0.058 (3)		
RDM+gluc	1.58±0.15 (3)	0.466±0.033 (3)		
TRIS + acetate	0.38	0.189[c]	Forchhammer & Lindahl (Ref. (*45*))	
TRIS + succ	0.60	0.224		
TRIS + gluc	1.04	0.295		
TRIS + cAA+ gluc	1.46	0.421		
FL Broth	1.73	0.469		
Med. C + succ	0.42	0.200[d]	Bremer & Dennis (Ref. (*14*))	
Med. C + glyc	0.69	0.255		
Med. C + gluc	1.04	0.331		
Med. C +AA+ glyc	1.39	0.391		
Med. C + AA+gluc	1.73	0.471		

a. Abbreviations: **M63+glyc** – Miller's M63 (*10*) +0.5% (v/v) glycerol; **M63+gluc** - M63+0.5% (w/v) glucose; **cAA+glyc** - M63+0.5% (v/v) glycerol+0.2% (w/v) casamino acids; **cAA+gluc** - M63+0.5% (w/v) glucose+0.2% (w/v) casamino acids; **RDM+glyc** - Neidhardt's rich defined media (*11*) +0.5% (v/v) glycerol; **RDM+gluc** - Neidhardt's rich defined media+0.5% (w/v) glucose; **TRIS** – Tris buffered with 0.2% of the indicated carbon source; **TRIS+cAA** – TRIS buffer with 0.75% (w/v) casamino acids; **FL Broth** – TRIS buffer with 0.2% glucose, 1% meat extract, 1% peptone and 0.5% yeast extract; **Med. C** – Phosphate buffer with 0.2% (w/v) of the indicated carbon source (*46*); **Med. C +AA** – Medium C supplemented with all amino acids >50 µg/ml, in proportion to the molar concentrations in *E. coli* protein.
b. Error is displayed as ± standard deviation among replicates. Number of replicates (done on different days) is shown in parentheses.
c. Using the estimate that 86% of total RNA is rRNA (*13*).
d. Using the estimate that there are 5.6×10^{15} amino acid residues per µg of protein, and that the average molecular weight of an RNA nucleotide is 324 (*14*).

Table S2 - Experimental data and error estimates for translational mutants derived from Xac

The parent strain Xac, and the mutants derived from this strain, UK285 (SmR) and UK317 (SmP), are proline/arginine auxotrophs. All growth media for these strains contain 10mM proline and 2.5mM arginine, in addition to any other nitrogen sources listed. Data appears in Fig. 1B.

Medium[a]	Xac	
	Growth rate λ (/h)[b]	RNA/protein (µg/µg)
cAA+gluc	1.03±0.04 (8)	0.302±0.043 (8)
+2 µM Cm[c]	0.94±0.01 (2)	0.379±0.073 (2)
+4 µM Cm	0.79±0.01 (2)	0.383±0.035 (2)
+8 µM Cm	0.47±0.10 (2)	0.458±0.005 (2)
+12 µM Cm	0.26±0.09 (2)	0.481±0.011 (2)
cAA+glyc	0.83±0.03 (2)	0.278±0.028 (8)
M63+gluc	0.60±0.01 (2)	0.199±0.027 (6)
M63+glyc	0.54±0.01 (2)	0.195±0.016 (6)

Medium[a]	UK285 (SmR)		UK317 (SmP)	
	Growth rate λ (/h)	RNA/protein (µg/µg)	Growth rate λ (/h)	RNA/protein (µg/µg)
cAA+gluc	0.82±0.02 (5)	0.414±0.066 (5)	0.57±0.02 (4)	0.468±0.064 (4)
cAA+glyc	0.71±0.04 (3)	0.350±0.027 (3)	0.45±0.03 (6)	0.418±0.062 (6)
M63+gluc	0.62±0.09 (4)	0.318±0.046 (4)	0.44±0.01 (3)	0.347±0.050 (3)
M63+glyc	0.47±0.10 (4)	0.254±0.061 (4)	0.33±0.07 (3)	0.311±0.042 (3)

a. All media based on Miller's M63 (see SOM Methods), supplemented with proline/arginine. **M63+glyc** – Miller's M63 +0.5% (v/v) glycerol; **M63+gluc** - M63+0.5% (w/v) glucose; **cAA+glyc** - M63+0.5% (v/v) glycerol+0.2% (w/v) casamino acids; **cAA+gluc** - M63+0.5% (w/v) glucose+0.2% (w/v) casamino acids;
b. Error is displayed as ± standard deviation among replicates. Number of replicates (done on different days) is shown in parentheses.
c. **Cm** – chloramphenicol
d. NA – Not applicable.

The translational capacities (κ_t from Eq. [1]) were fit to the data in Fig. 1B using weighted-least squares to account for error in the growth rate and RNA/protein measurements (*47*),

Strain	Translational capacity κ_t (µg protein/ µg RNA / h)	Measured elongation rate (a.a./s) (Ref. (*3*))
Xac	4.0±1.2	15
SmR	2.3±1.4	7.8
SmP	1.47±0.88	5

Table S3 – Experimental data and error estimates for Fig. 2AC

Medium[a]	Strain EQ2		Strain EQ3[b]	
	Growth rate λ (/h)[c]	RNA/protein (μg/μg)	Growth rate λ (/h)	β-gal/protein[d] ϕ_Z (μg/μg)
M63+glyc	0.40±0.03 (2)	0.177±0.006 (2)	0.40±0.02 (6)	0.082±0.006 (6)
+2 μM Cm[e]	0.33±0.01 (2)	0.291±0.014 (2)	0.35±0.01 (6)	0.052±0.005 (6)
+4 μM Cm	0.24±0.01 (2)	0.375±0.015 (2)	0.26±0.01 (6)	0.041±0.002 (6)
+8 μM Cm	0.19±0.03 (2)	0.414±0.028 (2)	0.15±0.02 (6)	0.024±0.006 (6)
+12 μM Cm	0.12±0.01 (2)	0.631±0.092 (2)	0.11±0.01 (6)	0.016±0.012 (6)
M63+gluc	0.57±0.02 (5)	0.230±0.014 (2)	0.57±0.02 (6)	0.067±0.008 (6)
+2 μM Cm	0.50±0.02 (5)	0.303±0.009 (4)	0.48±0.01 (6)	0.061±0.006 (6)
+4 μM Cm	0.39±0.04 (5)	0.371±0.009 (4)	0.38±0.02 (6)	0.050±0.003 (6)
+8 μM Cm	0.30±0.02 (5)	0.400±0.072 (4)	0.21±0.10 (6)	0.032±0.013 (6)
+12 μM Cm	0.23±0.03 (4)	0.496±0.051 (4)	0.20±0.09 (6)	0.025±0.005 (6)
cAA+glyc	0.71±0.03 (4)	0.224±0.029 (3)	0.70±0.03 (6)	0.057±0.003 (6)
+2 μM Cm	0.57±0.03 (4)	0.313±0.037 (3)	0.50±0.01 (6)	0.036±0.005 (6)
+4 μM Cm	0.38±0.01 (4)	0.435±0.045 (2)	0.36±0.01 (6)	0.032±0.009 (6)
+8 μM Cm	0.23±0.04 (4)	0.473±0.042 (2)	0.19±0.02 (6)	0.013±0.009 (6)
+12 μM Cm	0.14±0.01 (3)	0.524±0.079 (2)	0.10±0.03 (6)	0.007±0.003 (6)
cAA+gluc	1.00±0.05 (5)	0.287±0.009 (3)	0.90±0.04 (6)	0.054±0.003 (6)
+2 μM Cm	0.87±0.05 (5)	0.340±0.012 (3)	0.78±0.04 (3)	0.046±0.003 (3)
+4 μM Cm	0.67±0.04 (5)	0.374±0.015 (2)	0.60±0.03 (3)	0.040±0.004 (3)
+8 μM Cm	0.43±0.06 (5)	0.471±0.028 (2)	0.45±0.04 (3)	0.031±0.002 (3)
+12 μM Cm	0.28±0.05 (5)	0.577±0.013 (4)	0.32±0.03 (3)	0.019±0.002 (3)
RDM+glyc	1.31±0.07 (3)	0.414±0.058 (3)	1.33±0.05 (6)	0.034±0.008 (6)
+2 μM Cm	0.90±0.13 (2)	0.476±0.063 (3)	0.68±0.04 (4)	0.016±0.012 (4)
+4 μM Cm	0.46±0.01 (3)	0.618±0.081 (3)	0.45±0.05 (4)	0.010±0.005 (4)
+8 μM Cm	0.20±0.04 (3)	0.715±0.065 (3)	0.24±0.03 (4)	0.011±0.005 (4)
+12 μM Cm	0.11±0.03 (3)	0.785±0.100 (3)	0.23±0.07 (4)	0.010±0.004 (4)
RDM+gluc	1.58±0.15 (3)	0.466±0.033 (3)	1.66±0.05 (6)	0.022±0.002 (6)
+2 μM Cm	1.18±0.10 (3)	0.500±0.037 (3)	1.22±0.07 (4)	0.016±0.005 (4)
+4 μM Cm	0.89±0.08 (3)	0.584±0.050 (3)	0.89±0.07 (4)	0.012±0.002 (4)
+8 μM Cm	0.31±0.12 (3)	0.691±0.114 (3)	0.43±0.04 (4)	0.008±0.004 (4)
+12 μM Cm	0.13±0.02 (3)	0.769±0.029 (3)	0.24±0.02 (4)	0.009±0.004 (4)

a. Abbreviations: **M63+glyc** - M63+0.5% (v/v) glycerol; **M63+gluc** - M63+0.5% (w/v) glucose; **cAA+glyc** - M63+0.5% (v/v) glycerol+0.2% (w/v) casamino acids; **cAA+gluc** - M63+0.5% (w/v) glucose+0.2% (w/v) casamino acids; **RDM+glyc** - Neidhardt's rich defined media+0.5% (v/v) glycerol; **RDM+gluc** - Neidhardt's rich defined media +0.5% (w/v) glucose.

b. EQ2 and EQ3 exhibit the same growth rate and RNA/protein ratio for a given growth medium.

c. Error is displayed as ± standard deviation among replicates. Number of replicates (done on different days) is shown in parentheses.

d. β-galactosidase (LacZ) activity measured using a modification of Miller's assay (see SOM Methods). Activity was converted to μg of β-galactosidase enzyme (lyophilized powder, Sigma), and normalized to total protein (Bovine Serum Albumin (BSA) used as the standard).

e. **Cm** – chloramphenicol.

Table S4 – Phenomenological parameters inferred from experimental data (Fig. 2A)

Medium[a]	Growth rate λ_0 (/h)	$r_{max} (\mu g / \mu g)$[b]	Linearity coefficient (r^2)[c]	$\phi_R^{max} (\mu g / \mu g)$[d]
M63+glyc	0.40±0.03	0.668±0.056	0.93	0.508±0.043
M63+gluc	0.57±0.02	0.670±0.066	0.96	0.509±0.050
cAA+glyc	0.71±0.03	0.613±0.053	0.98	0.466±0.040
cAA+gluc	1.00±0.05	0.668±0.030	0.96	0.508±0.023
RDM+glyc	1.31±0.07	0.773±0.058	0.96	0.587±0.044
RDM+gluc	1.58±0.15	0.793±0.032	0.97	0.603±0.024
Average	NA[h]	0.72±0.13	NA	0.547±0.099

Medium[a]	$\phi_Q (\mu g / \mu g)$[e]	λ_c (/h)[f] (Eq. [5])	$\phi_c (\mu g / \mu g)$[g] (Eq. [6])	κ_n (µg/µg/h)[b]
M63+glyc	0.492±0.043	2.61±0.28	0.44±0.04	0.85±0.14
M63+gluc	0.491±0.050	2.62±0.32	0.44±0.05	1.32±0.23
cAA+glyc	0.534±0.040	2.37±0.26	0.40±0.04	1.86±0.34
cAA+gluc	0.492±0.023	2.61±0.18	0.44±0.02	2.54±0.26
RDM+glyc	0.413±0.044	3.09±0.30	0.52±0.04	3.45±0.83
RDM+gluc	0.397±0.024	3.18±0.21	0.54±0.03	4.44±0.69
Average	0.453±0.099	2.85±0.60	0.48±0.10	NA

a. Abbreviations: **M63+glyc** - M63+0.5% (v/v) glycerol; **M63+gluc** - M63+0.5% (w/v) glucose; **cAA+glyc** - M63+0.5% (v/v) glycerol+0.2% (w/v) casamino acids; **cAA+gluc** - M63+0.5% (w/v) glucose+0.2% (w/v) casamino acids; **RDM+glyc** - Neidhardt's rich defined media+0.5% (v/v) glycerol; **RDM+gluc** - Neidhardt's rich defined media+0.5% (w/v) glucose.

b. Slope and y-intercept ($1/\kappa_n$ and r_{max}, respectively, from Eq. [2]) were fit to the data in Fig. 2A using weighted-least squares to account for error in the growth rate and RNA/protein measurements (*47*). Error is displayed as ± the error associated with the linear fit.

c. Linearity coefficient from the straight-line fit used to determine r_{max}.

d. $\phi_R^{max} = \rho \cdot r_{max} (\rho = 0.76)$; see Eq. [S1].

e. $\phi_Q = 1 - \phi_R^{max}$.

f. From Eq. [5], $\lambda_c = \kappa_t \cdot (r_{max} - r_0)$. Error is displayed as ± the error propagated from the individual errors in κ_t, r_{max} and r_0.

g. From Eq. [6], $\phi_c = \rho \cdot (r_{max} - r_0)$. Error is displayed as ± the error propagated from the individual errors in r_{max} and r_0.

h. NA – Not applicable.

Table S5 - Translational inhibition –
Other antibiotics and historical data (Fig. S2)

Medium[a]	Growth rate λ (/h)	RNA/protein (μg/μg)	Source	Symbol
glc+cAA	0.96	0.38	This study	▲
+0.5 µM Tet[b]	0.91	0.40		
+1 µM Tet	0.70	0.46		
+2 µM Tet	0.56	0.47		
+4 µM Tet	0.17	0.70		
glyc+cAA	0.75	0.31	This study	▲
+0.5 µM Tet	0.60	0.37		
+1 µM Tet	0.42	0.38		
+2 µM Tet	0.28	0.56		
+4 µM Tet	0.15	0.61		
glc+cAA	0.98	0.34	This study	▼
+2 µg/µL Kan	0.89	0.35		
+4 µg/µL Kan	0.92	0.34		
+8 µg/µL Kan	0.67	0.40		
glc minimal (30°C)	0.667	0.325	Harvey and Koch (Ref. (*16*))	△
+0.5 µM Cm	0.593	0.384		
+1 µM Cm	0.524	0.413		
+2 µM Cm	0.361	0.454		
+3 µM Cm	0.305	0.585		
+4 µM Cm	0.190	0.622		
+6 µM Cm	0.125	0.640		
MOPS+AA	1.05	0.38	Cole et al. (Ref. (*41*))	○
MOPS+AA	1.05	0.37		
+0.001 mM IPTG	0.97	0.42		
+0.001 mM IPTG	0.96	0.42		
+0.01 mM IPTG	0.90	0.39		
+0.01 mM IPTG	0.86	0.41		
+0.03 mM IPTG	0.69	0.52		
+0.03 mM IPTG	0.63	0.50		
+0.1 mM IPTG	0.52	0.57		
+1.0 mM IPTG	0.39	0.62		
MOPS+AA	1.13	0.37	Olsson et al. (Ref. (*42*))	○
+ 0.07 mM IPTG	1.08	0.36		
+ 0.08 mM IPTG	1.04	0.36		
+ 0.09 mM IPTG	0.94	0.42		
+ 0.10 mM IPTG	0.92	0.41		
+ 0.50 mM IPTG	0.65	0.46		
+ 1.00 mM IPTG	0.38	0.58		

Table S5 (cont.)

Transcription inhibition using rifampicin (Fig. S2)

Medium	Growth rate λ (/h)	RNA/protein ($\mu g/\mu g$)	Source	Symbol
glyc+cAA	0.78	0.25		
+6 µM Rif	0.57	0.27		
+8 µM Rif	0.40	0.26	This study	■
+10 µM Rif	0.30	0.24		
+12 µM Rif	0.15	0.24		
glycerol	0.40	0.17		
+6 µM Rif	0.30	0.19		
+8 µM Rif	0.21	0.21	This study	◆
+10 µM Rif	0.09	0.22		
+12 µM Rif	0.06	0.21		

a. Abbreviations: **M63+glyc** - M63+0.5% (v/v) glycerol; **M63+gluc** - M63+0.5% (w/v) glucose; **cAA+glyc** - M63+0.5% (v/v) glycerol+0.2% (w/v) casamino acids; **cAA+gluc** - M63+0.5% (w/v) glucose+0.2% (w/v) casamino acids; **RDM+glyc** - Neidhardt's rich defined media +0.5% (v/v) glycerol; **RDM+gluc** - Neidhardt's rich defined media +0.5% (w/v) glucose.; **glc minimal** – phosphate buffered medium with glucose and NH_4^+, supplemented with several amino acids and vitamins (see Ref. (*16*) for details); **MOPS+AA** – MOPS buffered medium with glucose and NH_4^+, supplemented with amino acids and vitamins (see Refs. (*41, 42*) for details).
b. **Tet** – tetracycline; **Kan** – kanamycin; **Cm** – chloramphenicol; **IPTG** – Isopropyl β-D-1-thiogalactopyranoside; **Rif** – rifampicin.

Table S6 – Data in Fig. S4

Both mutant strains (EQ3 and EQ39) express LacZ from a PLtetO1 promoter on the chromosome (see SOM Methods), but the autoregulated strain (EQ39) includes a negative feedback loop provided by PLtetO1-*tetR*, where TetR is the tet-repressor inhibiting PLtetO1.

Nutrient limitation					
	EQ39 (negative autoregulation)		Medium	EQ3 (constitutive expression)	
Medium[a]	Growth rate λ (/h)	β-gal/protein[b] (μg/μg)		Growth rate λ (/h)	β-gal/protein (μg/μg)
RDM+gluc	1.39	0.0052	RDM+gluc	1.65	0.020
RDM+glyc	1.15	0.0059	RDM+glyc	1.30	0.036
cAA+glyc	0.82	0.0055	cAA+gluc	0.90	0.054
M63+glyc	0.44	0.0063	cAA+glyc	0.70	0.057
Glycine	0.26	0.0054	M63+gluc	0.57	0.067
			M63+glyc	0.40	0.082

Translational limitation					
	EQ39 (negative autoregulation)		Medium	EQ3 (constitutive expression)	
Medium	Growth rate λ (/h)	β-gal/protein (μg/μg)		Growth rate λ (/h)	β-gal/protein (μg/μg)
cAA+gluc	0.96	0.0043	cAA+gluc	0.90	0.054
+4 μM Cm[c]	0.61	0.0048	+2 μM Cm	0.78	0.046
+8 μM Cm	0.46	0.0044	+4 μM Cm	0.60	0.040
+10 μM Cm	0.33	0.0043	+8 μM Cm	0.45	0.031
+12 μM Cm	0.27	0.0046	+12 μM Cm	0.32	0.019

a. Abbreviations: **Glycine** – M63-based (with 20 mM glycine as the sole nitrogen source) +0.5% (v/v) glycerol; **M63+glyc** - M63+0.5% (v/v) glycerol; **M63+gluc** - M63+0.5% (w/v) glucose; **cAA+glyc** - M63+0.5% (v/v) glycerol+0.2% (w/v) casamino acids; **cAA+gluc** - M63+0.5% (w/v) glucose+0.2% (w/v) casamino acids; **RDM+glyc** - Neidhardt's rich defined media+0.5% (v/v) glycerol; **RDM+gluc** - Neidhardt's rich defined media +0.5% (w/v) glucose. 20ng/ml of the inducer chlortetracycline (cTc) was added to the growth medium for EQ39 (*6*).
b. β-galactosidase (LacZ) activity measured using a modification of Miller's assay (see SOM methods). Activity was converted to μg of β-galactosidase enzyme (lyophilized powder, Sigma), and normalized to total protein (BSA standard).
c. **Cm** – chloramphenicol.

Table S7 - Table of bacterial strains used in this study

Strain	Genotype	Derived From	Comments	Origin
EQ1	MG1655 wild type		Wildtype	F. R. Blattner
TK200	$\Delta lacI$ $\Delta lacY$	EQ1	Constitutive LacZ	Kuhlman *et al.* (*48*)
EQ2	$\Delta lacI$ $\Delta lacY$ $\phi(sp^r\text{-}tetR\text{-}lacI^q)$	TK200	Constitutive LacI and TetR	This study.
EQ3	$\Delta lacI$ $\Delta lacY$ km^r:P_{LtetO1}-*lacZ* at the *lac* locus	EQ1	Constitutive LacZ	This study.
EQ39	$\Delta lacY$, $\Delta lacI$, km^r:*rrnB*T:P*LTet-O1-lacZ* at the *lac* locus, *bla*:P*LTet-O1-tetR* at the *attB* site	EQ1	LacZ regulated by TetR which is under negative feedback regulation	Klumpp *et al.* (*6*)
GQ6 (CH337)	XAC wild type $\Delta prolac$, *argE*(amber)*rpoB*, *gyrA*, Ara, *aroE* (Tn10)		Parent strain for translational mutants SmR and SmP	via Diarmaid Hughes (*2, 3*)
GQ8 (CH341) (UK285)	XAC rpsL141 Sm^r	XAC	Streptomycin resistant - SmR	via Diarmaid Hughes (*2, 3*)
GQ9 (CH349) (UK317)	XAC Sm^p	XAC	Streptomycin pseudoresistant - SmP	via Diarmaid Hughes (*2, 3*)
EQ30	$\Delta lacI$ $\Delta lacY$ $\Delta galK$ $\Delta ryhB$ $\phi(bla$- P_{LlacO1}-*dnxylR*) pZE32P*u-lacZ* pZS4Int1	EQ1	Over-expresses LacZ using an activator controlled by LacI	This study.
EQ23	$\Delta lacI$ $\Delta lacY$ $\Delta galK$ $\Delta ryhB$ $\phi(bla$- P_{LlacO1}-*dnxylR*) pZS4Int1	EQ1	Negative control for EQ30	This study.

All strains derived from K12 MG1655 strain of *Escherichia coli*.

References

1. R. Lutz, H. Bujard, *Nucleic Acids Res* **25**, 1203 (1997).
2. M. O. Olsson, L. A. Isaksson, *Mol Gen Genet* **169**, 251 (1979).
3. T. Ruusala, D. Andersson, M. Ehrenberg, C. G. Kurland, *EMBO J* **3**, 2575 (1984).
4. S. Warming, N. Costantino, D. L. Court, N. A. Jenkins, N. G. Copeland, *Nucleic Acids Res* **33**, e36 (2005).
5. K. A. Datsenko, B. L. Wanner, *Proc Natl Acad Sci U S A* **97**, 6640 (2000).
6. S. Klumpp, Z. Zhang, T. Hwa, *Cell* **139**, 1366 (2009).
7. J. Perez-Martin, V. de Lorenzo, *J Mol Biol* **258**, 575 (1996).
8. E. Levine, Z. Zhang, T. Kuhlman, T. Hwa, *PLoS Biol* **5**, e229 (2007).
9. L. Diederich, L. J. Rasmussen, W. Messer, *Plasmid* **28**, 14 (1992).
10. J. H. Miller, *Experiments in molecular genetics*. (Cold Spring Harbor Laboratory, Cold Spring Harbor, N.Y., 1972), pp. xvi, 466 p.
11. F. C. Neidhardt, P. L. Bloch, D. F. Smith, *J Bacteriol* **119**, 736 (1974).
12. S. Benthin, J. V. Nielsen, J., *Biotechnology Techniques* **5**, 39 (1991).
13. O. Maaløe, in *Biological Regulation and Development,* R. F. Goldberger, Ed. (Plenum Press, New York, N. Y., 1979), pp. 487–542.
14. H. Bremer, P. P. Dennis, in *Escherichia coli and Salmonella,* F. C. Neidhardt, Ed. (ASM Press, Washington, D.C., 2009).
15. V. Shen, H. Bremer, *J Bacteriol* **130**, 1098 (1977).
16. R. J. Harvey, A. L. Koch, *Antimicrob Agents Chemother* **18**, 323 (1980).
17. P. P. Dennis, *J Mol Biol* **108**, 535 (1976).
18. S. Pedersen, P. L. Bloch, S. Reeh, F. C. Neidhardt, *Cell* **14**, 179 (1978).
19. J. G. Howe, J. W. Hershey, *J Biol Chem* **258**, 1954 (1983).
20. K. Nath, A. L. Koch, *J Biol Chem* **245**, 2889 (1970).
21. R. Young, H. Bremer, *Biochem J* **160**, 185 (1976).
22. J. Keener, M. Nomura, in *Escherichia coli and Salmonella typhimurium: cellular and molecular biology,* F. C. Neidhardt, R. Curtiss, Eds. (ASM Press, Washington, 1996).
23. L. U. Magnusson, A. Farewell, T. Nystrom, *Trends Microbiol* **13**, 236 (2005).
24. M. Cashel, D. R. Gentry, V. J. Hernandez, D. Vinella, in *Escherichia coli and Salmonella typhimurium: cellular and molecular biology,* F. C. Neidhardt, R. Curtiss, Eds. (ASM Press, Washington, 1996).
25. V. J. Hernandez, H. Bremer, *J Biol Chem* **268**, 10851 (1993).
26. M. H. de Smit, J. van Duin, *Proc Natl Acad Sci U S A* **87**, 7668 (1990).
27. M. A. Savageau, *Biochemical systems analysis: Study of function and design in molecular biology*. (Addison-Wesley, 1977).
28. N. Nanninga, C. L. Woldringh, in *Molecular Cytology of Escherichia coli,* N. Nanninga, Ed. (Academic Press, London, 1985), pp. 259–318.
29. S. Cayley, M. T. Record, Jr., *J Mol Recognit* **17**, 488 (2004).
30. E. M. Airoldi *et al.*, *PLoS Comput Biol* **5**, e1000257 (2009).
31. D. A. Fell, *Biochem J* **286 (Pt 2)**, 313 (1992).
32. F. C. Neidhardt, J. L. Ingraham, M. Schaechter, *Physiology of the Bacterial Cell: A Molecular Approach*. (Sinauer, Sunderland, UK, 1990).
33. M. Csete, J. Doyle, *Trends Biotechnol* **22**, 446 (2004).
34. J. Stelling, U. Sauer, Z. Szallasi, F. J. Doyle, 3rd, J. Doyle, *Cell* **118**, 675 (2004).
35. J. Monod, *Ann. Rev. Microbiol.* **3**, 371 (1949).

36.   R. Rosset, R. Monier, J. Julien, *Biochem Biophys Res Comm* **15**, 329 (1964).
37.   D. G. Fraenkel, F. C. Neidhardt, *Biochim Biophys Acta* **53**, 96 (1961).
38.   C. M. Brown, A. H. Rose, *J Bacteriol* **97**, 261 (1969).
39.   F. A. Alberghina, E. Sturani, J. R. Gohlke, *J Biol Chem* **250**, 4381 (1975).
40.   J. R. Cook, *J Protozool* **10**, 436 (1963).
41.   J. R. Cole, C. L. Olsson, J. W. Hershey, M. Grunberg-Manago, M. Nomura, *J Mol Biol* **198**, 383 (1987).
42.   C. L. Olsson, M. Graffe, M. Springer, J. W. Hershey, *Mol Gen Genet* **250**, 705 (1996).
43.   B. M. Willumsen, University of Copenhagen (1975).
44.   B. L. Wanner, R. Kodaira, F. C. Neidhardt, *J Bacteriol* **130**, 212 (1977).
45.   J. Forchhammer, L. Lindahl, *J Mol Biol* **55**, 563 (1971).
46.   C. E. Helmstetter, *J Mol Biol* **24**, 417 (1967).
47.   M. Krystek, M. Anton, *Measurement Sci Tech* **18**, 3438 (2007).
48.   T. Kuhlman, Z. Zhang, M. H. Saier, Jr., T. Hwa, *Proc Natl Acad Sci U S A* **104**, 6043 (2007).